Comparing EPOS-4, EPOS-LHC, and SMASH for identified-hadron observables in the NICA energy range*

Murad Badshah[1†] Haifa I. Alrebdi[2‡] Sana Raza Khan[3] Muhammad Ajaz[4§]

[1]Department of Physics, Abdul Wali Khan University Mardan, Mardan 23200, Pakistan
[2]Department of Physics, College of Science, Princess Nourah bint Abdulrahman University, P.O. Box 84428, Riyadh 11671, Saudi Arabia
[3]Government Post Graduate College for Women Mardan, Mardan 23200, Pakistan
[4]Department of Physics, Faculty of Science, University of Tabuk, Tabuk 47913, Saudi Arabia

Abstract: We report a systematic generator-level study of identified-hadron production in minimum-bias Au+Au collisions at $\sqrt{s_{NN}} = 6$, 7, and 8 GeV using EPOS-LHC, EPOS-4, and SMASH. These frameworks represent different microscopic approaches, ranging from string/core-corona and hydrodynamic descriptions to purely hadronic transport. We compare rapidity distributions, transverse-momentum spectra, two-dimensional $p_T - y$ density maps, particle-yield ratios, and number-of-constituent-quark-scaled elliptic flow. Charged and neutral pions provide a relatively model-insensitive baseline dominated by bulk production and resonance feed-down, whereas $K^{\pm}$, protons, and Λ baryons exhibit stronger model dependence. The $p_T - y$ maps identify the longitudinal and transverse phase-space regions in which the model predictions diverge, although conclusions for rare strange particles are limited to statistically populated regions. Elliptic flow is presented as v_2/n_q versus transverse kinetic energy per constituent quark, $(m_T - m_0)/n_q$. All three models exhibit an approximately common trend at low and intermediate transverse kinetic energy, with the closest visual grouping in EPOS-LHC; deviations and statistical uncertainties increase at larger $(m_T - m_0)/n_q$. Because each sample contains 50,000 events, no quantitative conclusions are drawn from sparsely populated forward-rapidity or high-p_T regions. The results provide exploratory model baselines and identify strange-particle spectra, K^-/K^+, Λ/π^+, double-differential $p_T - y$ measurements, and identified-particle elliptic flow as priority observables in the NICA energy range.

Keywords: heavy ion collisions, NICA, EPOS-LHC, EPOS-4, SMASH, rapidity spectra, transverse momentum spectra, Elliptic flow, NCQ scaling

DOI: 10.1088/1674-1137/ae9922 **CSTR:** 32044.14.ChinesePhysicsC.50114110

I. INTRODUCTION

Relativistic collisions of heavy ions provide a unique means to investigate the properties of strongly interacting matter under extreme temperature and density conditions. The theory of strong interactions, Quantum Chromodynamics (QCD), predicts a rich phase structure for such matter. Lattice QCD computations have found that at low baryon chemical potential ($\mu_B \approx 0$), hadronic matter undergoes a smooth crossover to a deconfined quark-gluon plasma (QGP) at a critical temperature $T_c \approx 155$ MeV [1−3]. This has been experimentally verified at the Relativistic Heavy Ion Collider (RHIC) and the Large Hadron Collider (LHC), where matter exhibits collective hydrodynamic flow, partonic energy loss (jet quenching), strangeness enhancement, and long-range correlations, reflecting the creation of a strongly coupled QGP [4−8].

However, at large baryon density, corresponding to lower collision energies, theoretical predictions diverge. At sufficiently large baryon chemical potential, some theoretical scenarios predict that the crossover may turn into a first-order phase transition terminating at a critical endpoint [9−11]. Model studies and QCD-inspired methods indicate that this transition may indeed occur. One of the most important outstanding issues in the field is to establish the location of this transition line and the QCD critic-

Received 24 May 2026; Accepted 12 August 2026; Accepted manuscript online 13 August 2026

* This research was supported by Princess Nourah bint Abdulrahman University Researchers Supporting Project number (PNURSP2026R106), Princess Nourah bint Abdulrahman University, Riyadh, Saudi Arabia

† E-mail: murad_phy@awkum.edu.pk; muradbadshah25295@gmail.com (Corresponding author)
‡ E-mail: hialrebdi@pnu.edu.sa
§ E-mail: mnawab@ut.edu.sa (Corresponding author)

Content from this work may be used under the terms of the Creative Commons Attribution 3.0 licence. Any further distribution of this work must maintain attribution to the author(s) and the title of the work, journal citation and DOI. Article funded by SCOAP[3] and published under licence by Chinese Physical Society and the Institute of High Energy Physics of the Chinese Academy of Sciences and the Institute of Modern Physics of the Chinese Academy of Sciences and IOP Publishing Ltd

al point [12]. Because data are scarce and the matter is baryon dense, experimental progress in this regime is difficult.

Over the past 20 years, there have been tremendous advances in programs at current facilities. The CERN SPS investigated $\sqrt{s_{NN}} = 6-17$ GeV and found evidence of anomalies in strangeness production, fluctuations, and event-by-event observables [13]. HADES at GSI has also focused on lower energies ($\sqrt{s_{NN}} = 2-3$ GeV), including detailed measurements of hadronic spectra, flow, and dilepton production, which are needed as input to hadronic transport models [14]. At RHIC, a systematic study of $\sqrt{s_{NN}} = 7.7-62$ GeV has been carried out in the Beam Energy Scan (BES-I and BES-II) [15]. Results from STAR and PHENIX show that observables such as v_2, the kurtosis of net-proton distributions, and particle ratios exhibit non-monotonic behavior, which is expected to arise from critical behavior and changes in baryon transport [15−18].

Although significant progress has been made, the region $\sqrt{s_{NN}} = 4-11$ GeV remains relatively unexplored by contemporary experiments. This energy window corresponds to the highest net-baryon densities accessible in heavy-ion collisions before reaching the lower μ_B values accessible at higher energies. Here, the onset of deconfinement and the first-order phase transition are most likely to appear. This gap will be addressed by the upcoming NICA (Nuclotron-based Ion Collider fAcility) at JINR Dubna [19, 20]. NICA will accelerate heavy ions (Au, Bi) at $\sqrt{s_{NN}} = 4-11$ GeV with high luminosity and a modern detector package, enabling measurements of hadronic spectra, collective flow coefficients, strangeness yields, and fluctuations of conserved charges with unprecedented precision.

Theoretical modelling remains important, even though Au + Au data in the same energy window have already been obtained at RHIC in the BES program [15]. These measurements, for example net-proton fluctuations and flow observables in the collision energy range of $7.7-62.4$ GeV, provide the first constraints on the QCD phase structure in the region of high baryon density and motivate an extended program at NICA. In this work, we use our calculations for model-to-model comparison in the NICA energy range, rather than as a definitive benchmark against existing RHIC data. We aim to identify observables for which the three descriptions differ most strongly, so that future measurements at NICA, together with additional dedicated comparisons to RHIC BES data, can efficiently distinguish between hadronic and hybrid descriptions. Simulations can provide a baseline expectation, identify discriminating observables, and inform the analysis strategy to be developed for NICA results [21, 22]. Importantly, different theoretical approaches rely on different assumptions about the relevant degrees of freedom: purely hadronic transport models assume that the medium is an interacting hadron gas, whereas hybrid models include partonic string dynamics and hydrodynamic collective flow. By comparing predictions within such frameworks, it is possible to identify which features of the results are robust and which depend on model assumptions [23].

In this work, we perform a comparative study of three state-of-the-art theoretical models, EPOS-LHC, EPOS-4, and SMASH, to systematically compare hadronic observables at $\sqrt{s_{NN}} = 6, 7$, and 8 GeV. These models represent distinct modeling philosophies. EPOS-LHC is a hybrid event generator originally tuned to LHC data that uses a core-corona representation in which dense core segments are statistically hadronized with parameterized collective flow, whereas dilute corona segments hadronize through standard string fragmentation. Its modern successor, EPOS-4, incorporates improved viscous hydrodynamics, event-by-event fluctuations, and improved hadronization schemes. SMASH (Simulating Many Accelerated Strongly-interacting Hadrons) is a microscopic hadronic transport model, providing a purely hadronic starting point with no explicit partonic or hydrodynamic stage.

Both EPOS-LHC and EPOS-4 are used here as downward extrapolations of their standard tunes. In our Au + Au simulations at collision energies of 6, 7 and 8 GeV, we vary the beam energy but not the model parameters. It is noteworthy that, at these low energies, the predictions should be treated as exploratory rather than as descriptions of existing data. Moreover, SMASH is used as a pure hadronic transport model, not as a hydrodynamic or partonic stage, and thus the three frameworks represent conceptually different approaches.

Our observables of interest include rapidity (y) distributions, transverse momentum (p_T) spectra, two-dimensional $p_T - y$ correlations, elliptic flow scaling with the number of constituent quarks (NCQ scaling), and particle-yield ratios (π^-/π^+, K^-/K^+, $\bar{p}/p$, K^+/π^+, K^-/π^-, p/π^+, and Λ/π^+). These observables probe different aspects of the collision dynamics [24]. Baryon transport and baryon stopping are experimentally studied by the rapidity distributions. Transverse momentum spectra measure radial flow and hadronization. The $p_T - y$ maps show the joint longitudinal and transverse regions in which each model deposits particle yield and are used here as qualitative phase-space diagnostics. The NCQ-scaled flow comparison tests how closely the identified-particle results approach a common scaled trend under the same generator-level analysis prescription. The ratios of the particles are sensitive to strangeness enhancement, baryon-meson competition, as well as the chemical freeze-out conditions.

This work provides a detailed theoretical background to the NICA program by a methodical study of the observables of these three models and the identification of discriminators that are capable of differentiating between

the hadronic and hybrid dynamics. The findings identify the most promising observables that can serve as probes of the baryon-rich QCD medium, and they also establish the basis of future experimental validation.

II. MODELS DISCUSSION

A. General remarks

Theoretical descriptions of heavy-ion collisions generally proceed through several stages: initial nucleon-nucleon interactions, pre-equilibrium dynamics, bulk medium evolution, hadronization, and late-time hadronic interactions. The physical content of the predictions depends on how these stages are modeled.

The EPOS framework is based on the collective dynamics and microscopic fragmentation of strings, in the form of a core-corona picture. In the EPOS-LHC configuration adopted here, the dense core segments are hadronized statistically with parameterized collective flow, while the evolution of the EPOS-4 core is based on viscous hydrodynamics; the string fragmentation is used for the description of the dilute corona segments. Such different implementations allow for comparison of collective-like and string-like dynamics with the purely hadronic transport description given by SMASH. By contrast, hadronic transport models such as SMASH solve the Boltzmann equation using a test-particle Monte Carlo method with purely hadronic degrees of freedom in the present work, and do not include an explicit hydrodynamic or partonic phase in the setup used here, unlike EPOS-LHC/EPOS-4.

By comparing EPOS-LHC, EPOS-4, and SMASH, it becomes possible to evaluate collective effects, strangeness production, and baryon stopping in the presence of a medium modeled as either hybrid or purely hadronic. This is especially noteworthy in the NICA energy window, where hadronic and deconfined mechanisms may both be present.

B. EPOS-LHC

EPOS-LHC [25] is an event generator based on a Gribov-Regge multiple-scattering model with parton-based string construction. In this approach, a parton ladder is introduced in every parton-parton interaction and is interpreted as a color flux tube, or string. These strings carry energy and momentum and subsequently fragment into hadrons. All scattering processes are treated with energy-momentum conservation.

One of the key features of EPOS is the core-corona approach [26]. In high-density regions, overlapping strings merge to form a dense core. In dilute regions, string fragments are produced independently in the corona. This two-component treatment allows EPOS to interpolate between hydrodynamic-like behavior in heavy-ion collisions and simple string fragmentation in pp or pA collisions.

In the present work, we use the public EPOS-LHC tune [25] implemented in the CRMC package. In the default tune, as noted above, EPOS-LHC is based on the standard EPOS Gribov-Regge multiple-scattering scheme. Each elementary scattering is represented by a parton ladder realized as a flux tube (string). String segments in high-density regions are assigned to a "core", which is hadronized statistically using parameterized collective flow, while low-density "corona" segments hadronize via standard string fragmentation. This produces collective-like spectra and strangeness enhancement without the need for a full (3+1)D hydrodynamic evolution followed by a hadronic transport afterburner. In our simulations, we generate EPOS-LHC events via CRMC in this default configuration by specifying only the colliding system, the centre-of-mass energy, and the number of events; we do not attach any external hadronic afterburner such as UrQMD.

EPOS-LHC was designed for very high energies, but it can also be used at lower energies by extrapolation. By extrapolation, we mean that we vary the beam energy, but not the model parameters. At $\sqrt{s_{NN}} = 6-8$ GeV, the core fraction is lower than under LHC conditions, although moderate collective flow and strangeness enhancement are still included in the model. This has made it a convenient hybrid baseline model for the NICA regime.

C. EPOS-4

The latest version of the EPOS framework is EPOS-4 [27], which includes significant improvements to the hydrodynamic and hadronization stages. It was developed to provide a unified description of small and large systems over a wide range of collision energies, from several GeV to several TeV. Some of the key improvements of EPOS-4 over EPOS-LHC are:

Viscous hydrodynamics: EPOS-4 includes a full viscous hydrodynamic stage with realistic shear and bulk viscosities, which are required to obtain accurate flow observables.

Refined core-corona separation: The core-formation criteria and string-fusion dynamics are described more accurately, providing a more realistic picture of baryon stopping.

Enhanced hadronization scheme: EPOS-4 employs a more flexible hadronization process; both recombination and fragmentation are allowed.

Event-by-event fluctuations: With an improved treatment of fluctuations, EPOS-4 can reproduce higher-order flow harmonics and correlations. In EPOS-4, this improved treatment of fluctuations means that it generates event-by-event fluctuating initial conditions due to multiple parallel parton-ladder (Pomeron) scatterings, which lead to a fluctuating flux-tube/string configuration.

After the core-corona separation, it generates fluctuating hydrodynamic initial conditions for the core. This should not be regarded as a pure Monte-Carlo Glauber initialization of the energy density; a Glauber-like geometry may be involved in sampling nucleon configurations in nuclear collisions, but the fluctuations that govern the subsequent evolution are dominated by the multiple-scattering/flux-tube dynamics at microscopic scales and by the core-corona process [28].

Coupling to hadronic afterburners: EPOS-4 is readily coupled to modern hadronic afterburners. In our simulations, EPOS-4 is run with its standard hadronic cascade, i.e., with the UrQMD afterburner turned on.

These features make EPOS-4 more predictive in the intermediate-energy range. EPOS-4 generally gives harder p_T spectra, stronger baryon-to-meson enhancement, and higher strangeness yields than EPOS-LHC. At $6-8$ GeV, EPOS-4 predictions will show clear deviations from hadronic models, providing an early test of collectivity.

Previous, more comprehensive comparisons with STAR Au + Au data indicate that the default EPOS-4 tune gives a qualitatively reasonable description of identified-hadron spectra up to intermediate BES energies. However, at $\sqrt{s_{NN}} = 7.7$ GeV, it overpredicts low-p_T yields and produces spectra that are too soft to describe several species, and it would therefore require dedicated retuning to provide a quantitatively reliable description at this energy [29]. Moreover, a separate analysis comparing EPOS-4, EPOS-LHC, and Pythia 8.3 with STAR charged-pion, kaon, and p(anti-p) spectra at $\sqrt{s_{NN}}$=7.7 and 11.5 GeV was already performed by some of the current authors (Ref. [30, 31]), using the STAR centrality definition of BES as implemented in Rivet. That paper concluded that EPOS-4 provides the most consistent overall agreement among these three generators, especially in central events; however, in the most peripheral events, EPOS-4 shows noticeable differences for the particle species studied at these energies [30, 31].

D. SMASH

The Simulating Many Accelerated Strongly-interacting Hadrons (SMASH) model [32] is a microscopic hadronic transport model intended to describe heavy-ion collisions at low and intermediate energies. SMASH is a computer code that provides a microscopic, numerical implementation of the relativistic Boltzmann equation for hadrons and resonances [33].

$$\frac{\mathrm{d}f_i}{\mathrm{d}t} = C_i[f], \tag{1}$$

with f_i denoting the distribution of hadron species i, and C_i the collision integral over all allowed scattering and decay processes.

SMASH includes the full spectrum of hadrons and resonances up to about 2.35 GeV. It evolves test particles through binary scatterings, resonance formation and decay, and mean-field effects (if enabled), using tabulated cross sections and decay channels. Where possible, its cross sections are constrained by experimental data. In addition, SMASH can include mean-field nuclear potentials, which are important at SIS energies in the context of collective flow.

Key features of SMASH: i) Resonance-based interactions: The majority of inelastic reactions proceed through resonance formation and decay. ii) Detailed hadronic rescattering: Final-state hadrons undergo multiple rescatterings, redistributing energy and shaping the spectra. iii) No partonic stages: When used as a stand-alone model, SMASH lacks deconfined degrees of freedom and hydrodynamics. Any collectivity arises solely from rescattering. iv) Versatility: In the present work, we use SMASH as a pure hadronic transport model; however, it has also been applied as a hadronic afterburner in hybrid schemes, including the SMASH-vHLLE hybrid scheme [34] and related low-energy schemes [35], which are directly applicable to NICA/BES energies. As a purely hadronic baseline, SMASH serves as an essential reference point. It is predicted to exhibit strong baryon stopping, broad proton rapidity distributions, and steeply falling p_T distributions in the $6-8$ GeV regime. A comparison of the SMASH and EPOS models highlights the importance of partonic and collective dynamics.

E. Modeling Philosophy of intermediate energies

The three models are not only technically different, but also rest on different philosophical assumptions regarding the active degrees of freedom at intermediate energies ($\sqrt{s_{NN}} = 4-11$ GeV). EPOS-LHC and EPOS-4 presuppose that collective dynamics, hydrodynamic expansion, and string fusion are already important at these relatively low energies, albeit to a smaller degree than at RHIC or the LHC. They thus include mechanisms associated with early pressure build-up, partonic collectivity, and enhanced strangeness production. In SMASH, by contrast, the medium is assumed to be a strongly interacting hadronic gas at all times. Any collective effects arise solely from rescattering among hadrons. This is a fundamental difference. Future NICA measurements of spectral shapes, strange-particle production, baryon-to-meson ratios, and identified-particle flow can constrain the different dynamical ingredients implemented in these models. However, no single one of these observables provides a unique determination of the microscopic degrees of freedom, and a combined comparison will be required. In this way, the use of these models in the NICA window makes it possible to test these competing theoretical philosophies in a direct manner.

III. RESULTS AND DISCUSSION

In this work, 50,000 Au + Au events were analyzed for each model and collision energy. The generator outputs were stored in HepMC format and processed with C++ analysis codes. Only final-state particles were used in all analyses, requiring status equal to 1. Identified particle species were selected by PDG codes. Transverse-momentum spectra were filled over p_T from 0 to 5 GeV/c (only $p_T \leq 3$ GeV/c is shown in the corresponding plots below; bins at higher p_T are generated in the analysis but are omitted from the plots due to limited or almost no statistics), and rapidity distributions over y from −3.5 to +3.5, where rapidity was computed from the particle four-momentum as $y = 0.5\ \ln[(E + p_z)/(E - p_z)]$, with safeguards for numerically ill-defined cases.

One-dimensional distributions were normalized per event and per bin width, producing per-event differential yields, whereas the two-dimensional $y - p_T$ maps were normalized per event only. Particle ratios were computed as bin-by-bin divisions of the corresponding normalized p_T spectra. The minimum-bias character of the samples is defined at the generator level: EPOS-4 was run with centrality set to 0, and SMASH sampled impact parameter over $b = 0 - 15$ fm with areal ("quadratic") sampling. For EPOS-LHC generated through CRMC, the collision is set to minimum bias by default.

The available event samples provide good statistical precision for dominant particles in the populated regions of phase space but are more limited for rare strange particles, forward-rapidity tails, high-p_T ratios, and the largest-KE_T/n_q flow points. Generating substantially larger EPOS-4 samples with the complete hydrodynamic evolution and hadronic cascade was computationally prohibitive within the available resources. Accordingly, we compare all three models using the same 50,000-event sample size and restrict quantitative conclusions to continuously populated regions with controlled statistical uncertainties. Sparse forward-rapidity kaon and Λ points, high-p_T tails, isolated cells of the two-dimensional maps, and the largest-KE_T/n_q flow points are shown only as qualitative indications of the accessible model phase space.

The rapidity distributions and the $p_T - y$ maps were histogrammed over $-3.5 < y < 3.5$. No additional rapidity or pseudorapidity restriction was applied to the original one-dimensional p_T spectra, particle ratios, or flow profiles; these quantities therefore represent inclusive generator-level results over the available final-state event record.

A. Rapidity distribution

Figure 1(a) shows the rapidity distribution of π^+ at $\sqrt{s_{NN}} = 6$ GeV predicted by EPOS-LHC, EPOS-4, and SMASH. The π^+ rapidity distribution at $\sqrt{s_{NN}} = 6$ GeV is reproduced nearly identically by SMASH, EPOS-LHC, and EPOS-4, with Gaussian-shaped [36] distributions of similar magnitude centered at midrapidity. This good agreement is not coincidental: at these energies, the vast majority of π^+ mesons are produced by resonance and higher baryonic-resonance decays, *e.g.*, $\Delta^{++} \to p\pi^+$ and $\Delta^+ \to n\pi^+$. Since these three models are similar in their treatment of resonance excitation and decay kinematics, the final-state π^+ distributions are correspondingly similar. Another reason is that pion multiplicities are much larger than those of other hadron species; therefore, statistical fluctuations or model-specific processes are largely washed out. The physical implication is that pion rapidity profiles are mainly sensitive to the overall energy-deposition mechanism and resonance-decay physics, both of which are strongly modeled in these approaches. This indicates that, although π^+ distributions confirm that the models respect energy and charge conservation, they do not strongly discriminate between hadronic-only transport (SMASH) and hybrid/string-based models (EPOS). Their role is therefore primarily as a reference rather than as a probe of new physics, because their behavior sets the scale against which kaons, protons, and hyperons are measured.

The π^- distribution, shown in Fig. 1(b), is similar to the π^+ distribution and exhibits nearly the same shapes and magnitudes across the models. The π^-/π^+ ratio is nearly unity as a function of rapidity, as expected in Au+Au collisions because of isospin symmetry [37]. At forward and backward rapidities, small deviations may occur due to the neutron excess in gold nuclei, although for the rapidity range studied these deviations are small. This is because π^- production also proceeds through resonance decays such as Δ^-, $N^* \to \pi^- + N$, where N^* is an excited nucleon state, and these channels are implemented similarly in all the models. The consistency of the descriptions of both π^+ and π^- indicates that charge conservation and resonance-decay chains are well implemented. Physically, this agreement implies that charged-pion yields at $\sqrt{s_{NN}} = 6$ GeV are dominated by trivial resonance feed-down rather than by processes sensitive to the initial stage of the collision. From a novelty perspective, this once again highlights the limitation of pions as probes: although they are abundant and experimentally accessible, they do not discriminate between transport and hybrid approaches. They are mainly useful as a standard baseline for comparing rarer species.

Please note that the EPOS-LHC model does not provide precise predictions for neutral pions in our calculations. This is not because the model suppresses π^0 production, but rather because it is a technical limitation of the public EPOS-LHC implementation. Since EPOS-LHC was originally optimized for high-energy LHC collisions, its output tables do not explicitly provide the neutral-pion yield; instead, neutral pions are reconstruc-

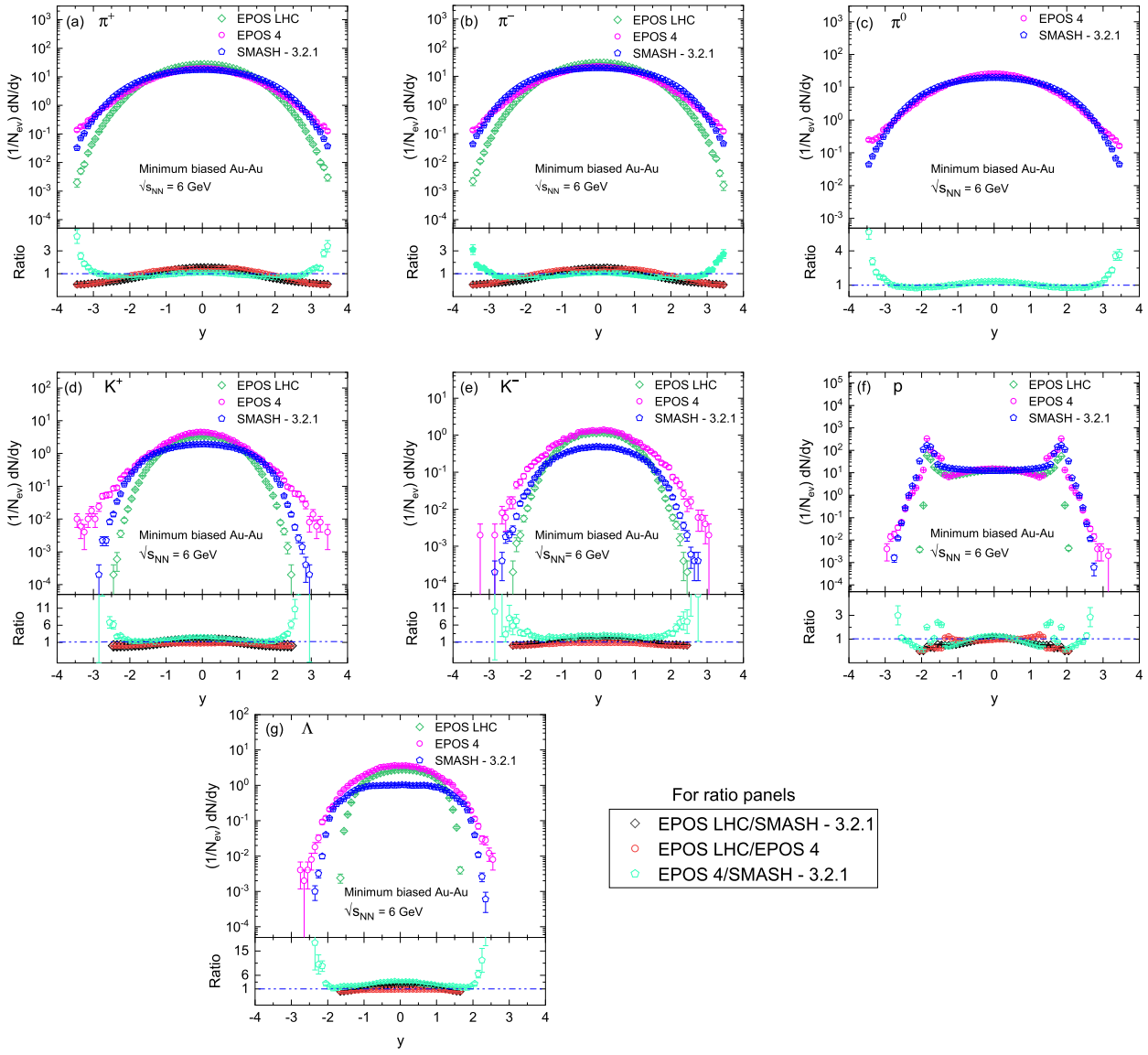


Fig. 1. (color online) Rapidity distributions (event-normalized dN/dy) of identified hadrons at minimum-bias in Au + Au collisions at $\sqrt{s_{NN}} = 6$ GeV forecasted by the three models. The results of EPOS-LHC, EPOS-4, and SMASH for various species of hadrons are presented in panels (a)-(g) to highlight the differences in total yield, width in rapidity, and mid-rapidity behaviour. Model legends are in the panels. Each plot has a ratio panel at its bottom, simplifying the model to model comparison.

ted indirectly through their electromagnetic decay channel ($\pi^0 \to \gamma\gamma$). By contrast, both EPOS-4 and SMASH treat π^0 as an explicit particle species in their event records: EPOS-4 as part of the extensive hadronic spectrum tuned to the FAIR/NICA energy scale, and SMASH through its detailed hadronic resonance and decay chains. For this reason, the comparison of the π^0 rapidity and transverse-momentum distributions in this work is limited to EPOS-4 and SMASH. The neutral-pion rapidity distributions at $\sqrt{s_{NN}} = 6, 7$ and 8 GeV, shown in panels (c) of Figs. 1−3, are generally consistent with those of charged pions and are broadly compatible with the corresponding charged-pion baseline.

The neutral-pion results are retained as a consistency check of isospin-related pion production and resonance-decay handling in EPOS-4 and SMASH. Their similarity to the charged-pion distributions confirms that the pion sector acts mainly as a bulk-production and resonance-feed-down baseline in the present energy range. We do not treat π^0 as an independent discriminator between the hadronic and hybrid descriptions, and none of the main conclusions depends on the neutral-pion result.

The model dependence is clear in the K^+ distribution, as seen in Fig. 1(d). EPOS-4 predicts visibly larger yields at midrapidity than SMASH and EPOS-LHC, which are closer to each other. The physical explanation is that K^+ production is dominated by associated production ($NN \to N\Lambda K^+$). The limitation on K^+ yields in SMASH is

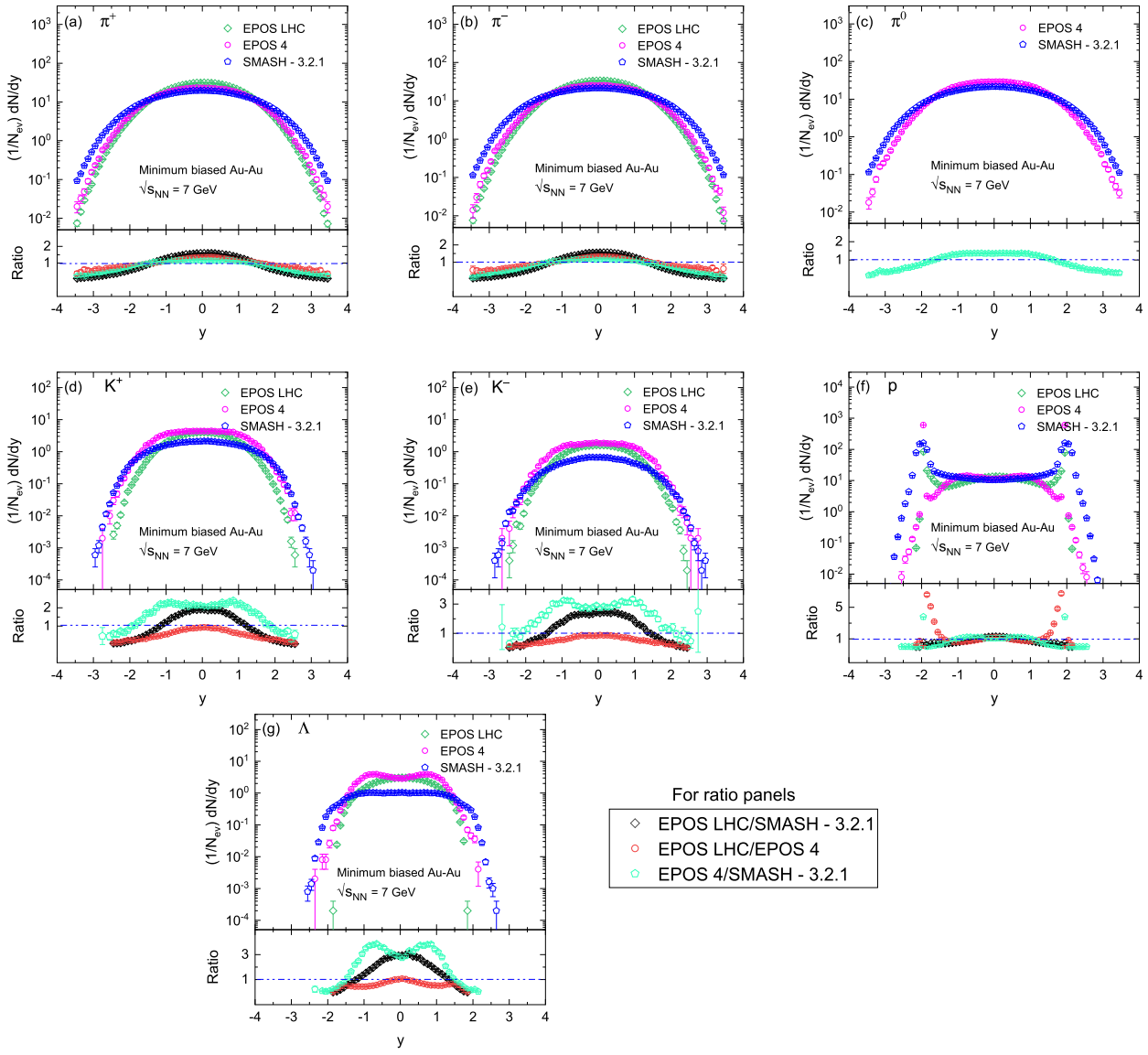


Fig. 2. (color online) Rapidity distributions (event-scaled $\mathrm{d}N/\mathrm{d}y$) of hadrons (identified) in minimum-bias Au + Au collisions, on a scale of $\sqrt{s_{NN}} = 7$ GeV. The three model predictions (EPOS-LHC, EPOS-4, SMASH) are illustrated to highlight the energy evolution between 6 and 7 GeV and model sensitivity in strange/higher-mass hadrons.

the presence of baryon-baryon near-threshold scatterings and the subsequent hadronic interactions. In comparison, EPOS-4 uses string fragmentation and a core-corona mechanism, which enables more efficient strangeness production and thus increases the K^+ yield. EPOS-LHC is tuned to higher energies and therefore shows intermediate behavior. This is a significant difference: K^+ is the first strange hadron species for which the models diverge, making it a sensitive probe of the extent to which the system is enhanced in strangeness. From a novelty standpoint, the fact that K^+ is already enhanced in EPOS-4 at $\sqrt{s_{NN}} = 6$ GeV suggests that strangeness enhancement may set in at lower energies than expected, which can be conclusively tested at NICA.

In Fig. 1(e), K^- production is strongly suppressed relative to K^+, and the suppression is strongest in SMASH. The dominant associated-production channel $NN \longrightarrow N\Lambda K^+$ produces K^+, not K^-. The $s\bar{s}$ pair-creation reactions, *e.g.* $\pi N \longrightarrow NK\bar{K}$, and the strangeness-exchange processes can instead yield the K^- mesons, and the final yields will be further modified by the absorption and rescattering of the K^- in baryon-rich matter. These reactions are energetically costly in baryon-rich environments, and $\sqrt{s_{NN}} = 6$ GeV is relatively low in this context. EPOS-4 predicts somewhat larger midrapidity K^- production, as string breakings provide an additional source of $s\bar{s}$ creation. EPOS-LHC again lies in between, with modest pair production. The separation among the

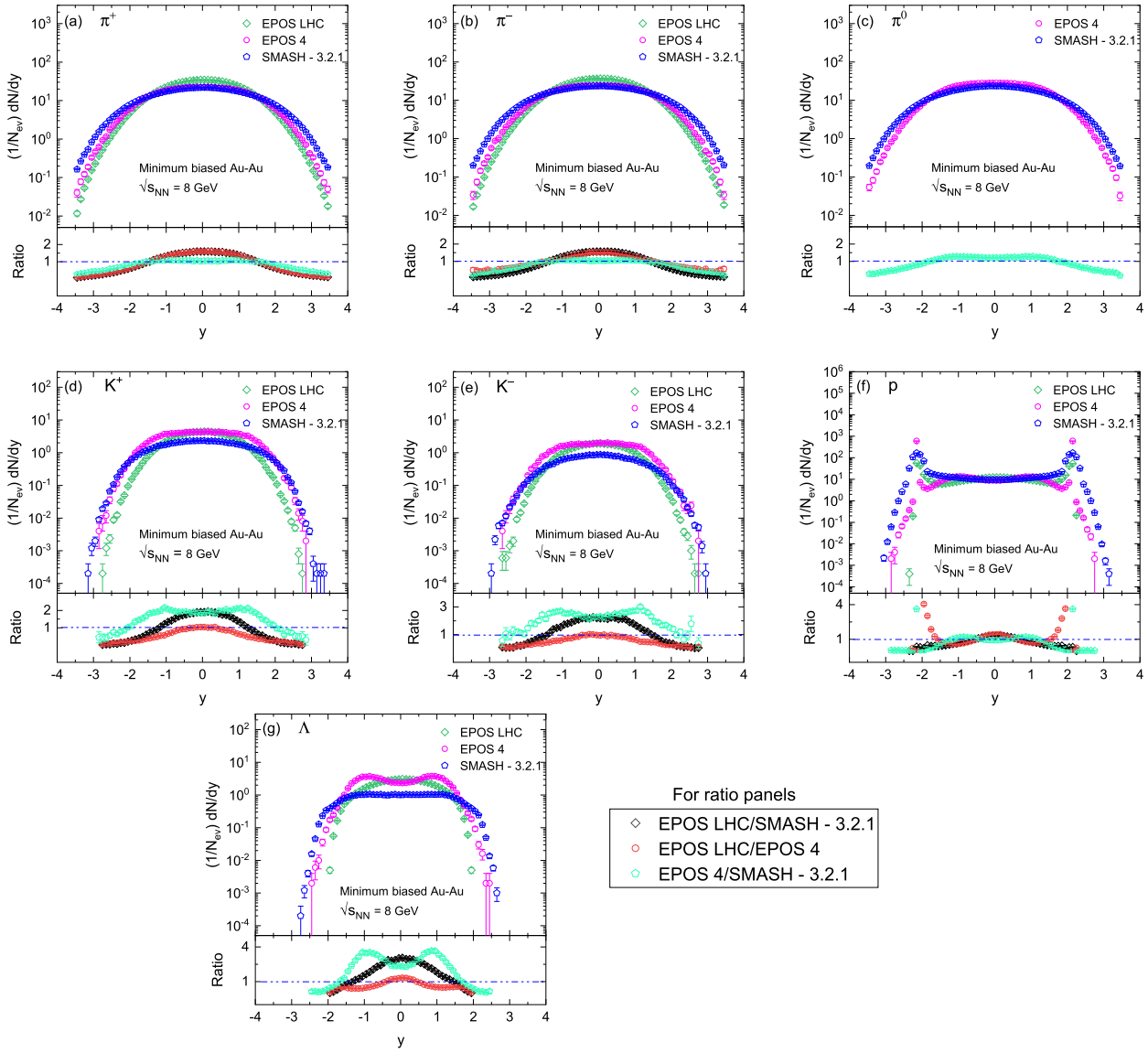


Fig. 3. (color online) Rapidity distributions (event-normalized $\mathrm{d}N/\mathrm{d}y$) of identified hadrons at minimum-bias in $\mathrm{Au}+\mathrm{Au}$ collisions at $\sqrt{s_{NN}} = 8$ GeV forecasted by the three models. The results of EPOS-LHC, EPOS-4, and SMASH for various species of hadrons are presented in panels (a)-(g) to highlight the differences in total yield, width in rapidity, and mid-rapidity behaviour. Model legends are in the panels.

models for K^- is important because these mesons are relatively heavy and therefore directly reflect the microscopic production mechanism. Physically, this is significant because K^- production probes the probability of pair creation, which depends very sensitively on the presence or absence of string-like dynamics. The novelty here is that the K^-/K^+ ratios at such energies are among the most sensitive tests of the production environment, and future NICA data can directly discriminate between hadronic and string-based pictures.

The proton $\mathrm{d}N/\mathrm{d}y$ at 6 GeV is shown in Fig. 1(f) and exhibits clear peaks in the fragmentation regions ($|y| \geq 1.5-2$), as well as a lower yield at midrapidity. The midrapidity yields of the three models are similar in magnitude; however, the fragmentation peaks differ clearly across the models. SMASH exhibits one of the widest rapidity distributions, with relatively large fragmentation yields and tails that extend closer to beam rapidity. That is, SMASH places a larger fraction of protons in the forward/backward rapidity regions than in midrapidity compared with some EPOS variants. EPOS-4 also generates sizeable fragmentation peaks and is close to SMASH in the fragmentation region, but its midrapidity yield is similar to that of SMASH. EPOS-LHC has the weakest fragmentation peaks among the three and a slightly narrower overall distribution; the forward/backward maxima of EPOS-LHC are smaller than those of SMASH and EPOS-4. Even at the low energy of 6 GeV, baryon stop-

ping remains important, although the models differ in the extent to which baryon number remains in the fragmentation regions. The broader distribution in SMASH arises because, in a microscopic hadronic cascade, baryons are more likely to undergo multiple scattering and resonance-mediated transport without the mechanisms that concentrate baryons in a narrow midrapidity region. EPOS-LHC, which is tuned to high energies, exhibits weaker fragmentation peaks in this regime, whereas EPOS-4, which is designed to handle intermediate energies more effectively, follows SMASH more closely in the fragmentation region.

The Λ rapidity distribution, shown in Fig. 1(g), also reflects differences in baryon stopping and strangeness production. EPOS-4 predicts a larger midrapidity Λ density than SMASH or EPOS-LHC. The physical explanation is that Λ production is closely linked to K^+ production through associated processes; as K^+ increases, Λ production also increases. In SMASH, Λ yields are constrained by hadronic scattering thresholds, and therefore are smaller. In EPOS-4, string fragmentation and partonic-like dynamics produce more Λs. This makes Λ particularly interesting: unlike protons, which are mainly sensitive to baryon transport, Λ production is sensitive to both baryon stopping and strangeness physics. The key point here is the strong model dependence of Λ yields at such low energies, which was less evident in previous SPS data. This shows that Λ measurements at NICA will provide a dual probe of baryon-charge redistribution and strangeness production.

In Fig. 2(a), the π^+ yield increases slightly in overall magnitude at $\sqrt{s_{NN}} = 7$ GeV, but the rapidity shape and model comparison remain the same as at 6 GeV. The three models again produce nearly identical Gaussian-shaped curves peaking at midrapidity, showing that pion yields are still dominated by resonance decays and bulk hadronic scattering. The physical explanation is unchanged: increasing $\sqrt{s_{NN}}$ by 1 GeV does not significantly alter the pion production mechanism; the system still spends most of its lifetime in the baryon-rich hadronic phase, where the Δ and N^* decays are the dominant channels. Accordingly, π^+ are not discriminants of microscopic physics but rather carriers of bulk entropy. The similarity among the models is significant because it shows that each model treats the conservation of soft bulk particles in a similar manner. However, this insensitivity also explains why pions are not adequate for distinguishing competing pictures of the early stage. The novelty here is the explicit demonstration that adding 1 GeV to $\sqrt{s_{NN}}$ in this energy window does not change the role of pions as baseline probes.

Figure 2(b) shows the π^- rapidity distribution, which again resembles that of π^+ and has a slightly higher yield than at 6 GeV, while the shapes remain almost model independent. The π^-/π^+ ratio remains near unity as a function of rapidity, indicating that isospin symmetry is preserved. This is because π^- production also arises strongly from resonance decays such as $\Delta^- \to n\pi^-$, and these channels are not sensitive to the small change in beam energy. The physical meaning is that charged-pion ratios at these energies measure global isospin equilibrium rather than finer collision dynamics. All models reproduce this behavior, which further confirms the reliability of their isospin conservation and resonance-feed-down implementations. As in the π^+ case, the novelty here is limited; the main point is to establish that the baseline is robust enough to interpret the results for strangeness and baryons.

The K^+ distribution, shown in Fig. 2(d), becomes larger and broader at 7 GeV than at 6 GeV. EPOS-4 yields much higher midrapidity values than SMASH, with EPOS-LHC in between. The physical explanation is that, with increasing $\sqrt{s_{NN}}$, associated production ($NN \to N\Lambda K^+$) becomes more frequent, and the string-based processes in EPOS-4 enhance this channel relative to the purely hadronic SMASH [38, 39]. This is directly connected to strangeness enhancement, where partonic or string-based processes increase strangeness yields more efficiently than hadronic scattering. In the literature, SPS experiments indicated a steep rise in the K^+/π^+ ratio with energy, the so-called horn, which has been attributed to the onset of deconfinement [40]. What is new in our results, however, is that in the $6-8$ GeV range the model differences in K^+ production are already dramatic, and NICA can use this observable as a sensitive probe of these processes.

Figure 2(e) shows the K^- rapidity distribution at 7 GeV, which increases relative to 6 GeV, but remains strongly suppressed compared with K^+. EPOS-4 is predicted to produce stronger K^- yields at midrapidity than SMASH, with EPOS-LHC taking an intermediate position. This is because an increase in $\sqrt{s_{NN}}$ opens up more phase space and production channels for K^- production, such as the creation of $s\bar{s}$ pairs, while SMASH is more limited by the hadronic thresholds, EPOS-4 can produce more strange pairs by string fragmentation. As a result, K^- production is sensitive to the efficiency of the $s\bar{s}$ pair formation [38, 39, 41], to strangeness-exchange processes, absorption, and rescattering in baryon-rich matter. The implication is that K^- is even more directly sensitive to the underlying microscopic degrees of freedom than K^+. This is novel in the sense that, even with a 1 GeV increase in $\sqrt{s_{NN}}$, the differences among the model predictions for K^- remain measurable, making this observable a top priority for future NICA analyses.

The double-hump structure remains present in the proton rapidity spectra at $\sqrt{s_{NN}} = 7$ GeV, as shown in Fig. 2(f). However, the fragmentation peaks tend to be higher than at 6 GeV (the plots show an increase in the forward/backward maxima with energy), and the midrapidity valley is slightly more filled in for some

models [42]. SMASH again exhibits a relatively broad proton rapidity distribution with prominent fragmentation peaks and long tails. Its width is larger than that of the EPOS curves (i.e., the yields at larger $|y|$ are higher in SMASH). EPOS-4 remains between SMASH and EPOS-LHC in the fragmentation region; in particular, the y bin at which EPOS-4 shows fragmentation peaks is similar to SMASH, although it can differ slightly depending on the specific y bin. EPOS-LHC has the narrowest distribution of the three, with smaller fragmentation peaks and a more flattened but less extended midrapidity shape. As $\sqrt{s_{NN}}$ increases, the longitudinal phase space becomes larger, and the models become more visibly different in their baryon-number distributions. Hadronic transport in SMASH causes additional protons to spread into the fragmentation regions. That behavior is partially reproduced by EPOS-4, which uses more realistic string/core dynamics at intermediate energies, whereas EPOS-LHC is the most concentrated at midrapidity (i.e., it has the least baryon flow into the fragmentation wings).

The Λ rapidity distribution, shown in Fig. 2(g), is largest at 7 GeV, with EPOS-4 yielding the highest values and SMASH the lowest. The physical explanation is that Λs, like K^+, are strongly affected by their associated production channels, which become more active as $\sqrt{s_{NN}}$ increases. This effect is enhanced by string dynamics in EPOS-4, but much less so in SMASH. The significance is that Λs provide a complementary probe to protons: protons measure baryon stopping, whereas Λs encode both stopping and strangeness production. From the literature perspective, enhanced Λ production was a classic SPS observation associated with strangeness enhancement [43–45], and our findings indicate that this behavior can already be observed in the 6 – 8 GeV region. The novelty is that model variations in Λ production are already strong at 7 GeV, making this species an obvious experimental target at NICA.

The increase in π^+ yields at 8 GeV, shown in Fig. 3(a), continues. However, the shape and inter-model consistency remain similar. The overlapping Gaussian-like profiles with peaked midrapidity appear in all models. The cause is the same, namely that resonance decays predominate in pion production despite the low-energy regime. Physically, this stability emphasizes that pion distributions do not reflect the microscopic dynamics of interest, but rather the generation of entropy. What is new is the confirmation that, across three successive energies, pions are nondiscriminating probes, and experiments should therefore focus on rarer hadrons to test the models.

The π^- distribution, shown in Fig. 3(b), is the same as that of π^+, except for a slightly higher yield than at 7 GeV, and the model-dependent shapes are nearly identical. The isospin-symmetric behavior is still reflected in the π^-/π^+ ratio, and no significant differences emerge. The physical meaning is again that pions are a consistency check rather than a discriminator. The only additional point is that the pion distributions remain robust throughout the 6 – 8 GeV window, which reinforces their role as baseline observables.

Figure 3(d) shows the K^+ rapidity distribution at $\sqrt{s_{NN}} = 8$ GeV. The model disagreement is most pronounced here: EPOS-4 predicts much higher midrapidity K^+ yields than SMASH and EPOS-LHC. This is because, as $\sqrt{s_{NN}}$ increases, the relevant production channels become more active, and the string mechanisms in EPOS enhance this effect, whereas SMASH remains constrained by hadronic scattering. Physically, this implies that strangeness enhancement is stronger in EPOS-4, which can be attributed to partonic-like dynamics. Importantly, even within this narrow energy range, the K^+/π^+ ratio, a typical SPS observable, is strongly model dependent [40]. The novelty is that K^+ production is one of the most effective observables for distinguishing hadronic and string-based mechanisms at NICA, as predicted by our simulations.

K^- yields further increase at 8 GeV, as shown in Fig. 3(e), but they remain suppressed relative to K^+. EPOS-4 gives the highest K^- yields, while SMASH gives the lowest. The physical reason is that the higher the value of $\sqrt{s_{NN}}$, the more phase space is available for the production of K^-, and EPOS string dynamics may further increase the production of $s\bar{s}$ pairs. This renders K^- a good tool to study strange-pair production and in-medium phenomena such as strange exchange, absorption, and rescattering. The implication is that the differences in K^- production are not only quantitative but also qualitative, as they reflect different microscopic mechanisms. What is new here is that, even in the low-energy regime, K^- distributions are highly model-dependent and therefore represent high-priority observables for NICA.

The proton rapidity spectra are most strongly hump-shaped at 8 GeV, as shown in Fig. 3(f). All three models yield very similar magnitudes at midrapidity, although the fragmentation asymptotes differ among the models. SMASH generates the most widespread distribution, with the highest relative yields in the fragmentation regions, though smaller than EPOS-4 at only two points, and the longest tails. SMASH shows the largest width enhancement over 6 – 8 GeV. EPOS-4 also exhibits substantial fragmentation peaks and is closer to SMASH than EPOS-LHC in the wings, with only modest differences in detail (the peak heights and absolute y positions are model dependent). EPOS-LHC is the narrowest and least peaked in the fragmentation regions; its midrapidity yields are similar to those of the other models, but it places less emphasis on the forward/backward maxima. Here, the separation between SMASH and EPOS-LHC is largest. The broadening of SMASH with energy suggests that baryons in a hadronic cascade are more likely to retain their

original longitudinal momentum and populate the fragmentation regions more heavily, whereas EPOS variants, especially EPOS-LHC, include mechanisms (core formation, string-junction dynamics, and stronger effective stopping in the model parametrization) that move more baryon density to midrapidity or at least reduce the weight of the fragmentation peaks.

The growth in Λ yields is even stronger at 8 GeV, as shown in Fig. 3(g), and EPOS-4 produces the largest increase compared with SMASH. The physical explanation is that the more Λs one has, the more frequent the associated production and fragmentation of strings become, favoring further Λ production. SMASH remains limited, resulting in fewer Λs overall. Physically, this demonstrates that Λ production is an integrated indicator of baryon transport and strangeness enhancement, and it is among the most informative species. From the literature perspective, Λ enhancement played a central role at SPS and RHIC in diagnosing strangeness physics. Our results are novel in that they show that Λ distributions differ strongly among models even within the $6-8$ GeV window, making this a sensitive probe for NICA.

B. Transverse momentum distributions

The π^+ production is shown in panel (a) of Fig. 4 as a function of p_T at 6 GeV (event-normalized, on a log scale). A clear hierarchy is observed: SMASH gives the steepest spectrum (the fastest fall-off with p_T), while EPOS-LHC and EPOS-4 produce flatter spectra at intermediate p_T (In the current energy scale, the range between 0.8 GeV/c and 2.5 GeV/c is the intermediate-p_T. The reason this was chosen is that below 0.8 GeV/c resonance feed-down and bulk freeze-out are a significant contribution to the spectra, and above 0.8 GeV/c collective and string dynamics start to make a greater contribution. At such energies, there exists no actual high-p_T domain in the RHIC/LHC sense, hence the range to a scale of about 3 GeV/c can be regarded as intermediate), with EPOS-LHC generally being the flattest of the three. The physical reason is that SMASH is a microscopic hadronic cascade, which generates pions mostly through resonance decays and limited rescattering; hence, it does not produce a strong radial push and yields fewer pions at intermediate p_T. The EPOS versions also feature string fragmentation and a collective core treatment, which can increase the transverse momentum, thus moving the yield to higher p_T and flattening the shape; in EPOS-LHC the core is treated by parameterized collective flow, whilst in EPOS-4 it is treated by viscous hydrodynamics. This separation is important since the intermediate-p_T region is sensitive to the transverse-momentum transfer process, which is influenced by the collective-like transverse processes: a flatter, more slowly falling spectrum corresponds to a larger effective inverse-slope parameter, which is compatible with stronger transverse-momentum transfer through radial expansion or string-related dynamics. This finding is consistent with slope analyses at these energies [46, 47], and the intermediate-p_T window is identified as the most discriminating region for pion spectra at NICA energies. A slope measurement in this region will distinguish hadronic from hybrid/string-inspired dynamics.

The same model ordering is observed in the π^- p_T spectrum at 6 GeV, shown in Fig. 4(b): SMASH, EPOS-4, and EPOS-LHC all exhibit steep spectra at higher p_T, and any numerical low-order variation is negligible. This can be explained by the same physical argument: resonance feed-down and weak rescattering in SMASH keep pions at low p_T, whereas the EPOS models extend this to pions with a finite amount of additional transverse momentum through core dynamics or string fragmentation. This panel supports the statement that intermediate-p_T charged pions are a sensitive probe of transverse dynamics in systems with rich particle species. It also shows that agreement at very low p_T does not imply identical physics; the discriminating power lies in the intermediate region.

The π^0 transverse-momentum distributions are displayed in panels (c) of Figs. 4–6, at $\sqrt{s_{NN}} = 6$ GeV, 7 GeV and 8 GeV, respectively. At 6 GeV, the p_T spectra fall steeply in SMASH, with most of the distribution concentrated in soft pions, $p_T < 1$ GeV/c, whereas EPOS-4 provides much flatter distributions extending into the intermediate region ($0.8-3$ GeV/c). This hardening reflects the inclusion of collective transverse expansion and string fragmentation in EPOS, which are absent in the hadronic-only SMASH. This trend continues at $\sqrt{s_{NN}} = 7$ GeV and 8 GeV, where the model differences increase in the high-p_T tail, i.e., $p_T > 1.3$ GeV/c, with increasing collision energy.

Much more explicit model dependence is observed in the K^+ transverse-momentum spectrum shown in Fig. 4(d). EPOS-4 yields higher overall multiplicities and a harder (flatter) spectral slope than SMASH, with EPOS-LHC lying between the two. The physical cause is that kaons are less resonance-dominated and are more strongly influenced by the production mechanism. In SMASH, threshold-limited associated production generates kaons, leading to steep spectra. In EPOS-4, additional channels include strings and partonic-like dynamics, so kaons have higher multiplicities and a larger radial push, resulting in flatter spectra. This is important because kaons are a clean probe of strangeness production and collective acceleration; therefore, kaon spectra directly test the physics assumptions of the models. Kaon spectra at SPS and BES energies are known to be sensitive probes of collectivity in baryon-rich matter. The new aspect here is that already at $\sqrt{s_{NN}} = 6$ GeV, kaons exhibit strong model separation, underscoring their significance as discriminators at NICA.

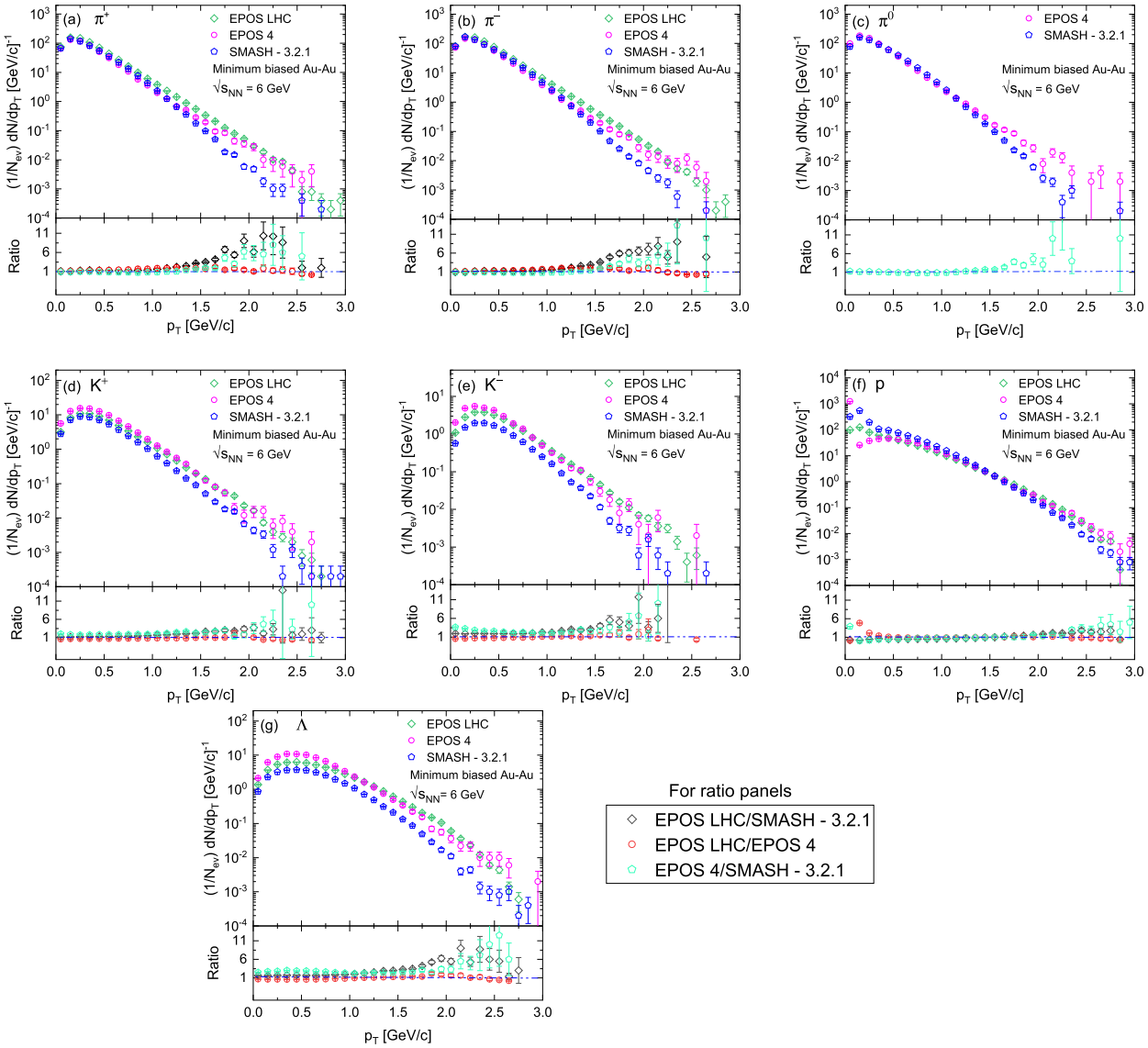


Fig. 4. (color online) Event-normalized $\mathrm{d}N/\mathrm{d}p_T$ transverse-momentum spectra of identified hadrons in minimum-bias Au + Au collisions at $\sqrt{s_{NN}} = 6$ GeV. The EPOS-LHC, EPOS-4, and SMASH model predictions are compared to demonstrate variations in the shape of the spectrum, slope (soft vs. hard components), and relative yield at low and intermediate p_T. Each plot has a ratio panel at its bottom, simplifying the model to model comparison.

The K^- p_T spectra in minimum-bias Au + Au collisions at $\sqrt{s_{NN}} = 6$ GeV are shown in Fig. 4(e). The strong suppression of the K^- spectra persists across models, although the shape and slope vary significantly. EPOS-4 predicts higher yields and a harder, more slowly falling spectrum, whereas SMASH predicts a lower-yield, more rapidly falling spectrum. This difference could be explained by their microscopic production mechanisms: string fragmentation and $s\bar{s}$ pair-production processes give an enhancement in EPOS, while they are less efficient in SMASH. The harder EPOS-4 spectrum might be a signature of other transverse-momentum generation from string-related and collective-like dynamics. Physically, this makes K^- especially sensitive to whether the system exhibits early partonic-like dynamics or is limited to hadronic processes. This is important because K^- spectra can directly reflect the level of strangeness equilibration in the system. The key point is that, at low $\sqrt{s_{NN}}$ where K^- yields are small, the spectral shape carries important information about the underlying dynamics, which is critical for NICA.

The proton p_T spectrum at 6 GeV, displayed in Fig. 4(f), shows noticeable model differences. SMASH produces steeper spectra, while EPOS-4 generates flatter distributions at intermediate p_T. The physical explanation is that in SMASH, protons retain much of their original momentum through hadronic scattering, with little collective acceleration, whereas in EPOS-4 the core-

corona picture induces radial flow in the core, resulting in a flatter spectrum. EPOS-LHC lies in between, as it is tuned as a hybrid model. This difference is important because both baryon transport and radial collectivity are encoded in proton spectra. Broader results from the RHIC BES demonstrated that baryon spectra hardened with energy, which can be interpreted as a manifestation of increasing collectivity. Such hardening is already expected to be observable in the 6 GeV region in EPOS-4, but not in SMASH, making proton spectra a decisive observable.

The strong enhancement of the proton distribution below approximately $p_T = 0.3\ \mathrm{GeV}/c$ should be interpreted with caution. The transverse-momentum spectra were constructed without an explicit rapidity or pseudorapidity restriction and therefore contain transported, stopped, fragmentation-region, and remnant-like baryons in addition to produced midrapidity protons. These baryons can retain substantial longitudinal momentum while carrying relatively small transverse momentum, thereby increasing the population of the first p_T bins. Resonance excitation and decay, elastic scattering, and the late hadronic stage may further modify this soft component. The present analysis does not separate these contributions quantitatively, and the very-low-p_T proton enhancement is therefore not used as an independent discriminator among the models.

We note that the differences in the low- and intermediate-p_T proton spectra between EPOS-LHC, EPOS-4, and SMASH are expected to be affected not only by their initial state and possible hydrodynamic dynamics, but also by their different treatment of the late hadronic stage. EPOS-4 features an explicit hadronic rescattering phase (UrQMD) following hydrodynamics. In contrast, SMASH incorporates hadronic transport throughout the entire evolution, while EPOS-LHC employs a parametrized approach for flow and resonance decays, without a separate transport afterburner. The baryon p_T spectra should therefore be regarded as a combined probe of early-time dynamics and the model-dependent hadronic phase.

Figure 4(g) displays the Λ p_T distribution in minimum-bias Au + Au collisions at 6 GeV. A clear difference among the three models is evident: SMASH has the steepest slope, while EPOS-4 and EPOS-LHC produce flatter, harder spectra, with EPOS-LHC being slightly harder than EPOS-4. This means that SMASH concentrates Λ production at low p_T, whereas the EPOS versions retain a larger population in the medium-p_T range ($0.8 - 3\ \mathrm{GeV}/c$). Physically, this reflects the production mechanisms: SMASH produces Λ baryons through associated hadronic processes (such as $NN \to N\Lambda K$) and through secondary rescattering, which is rarely able to generate large p_T. Conversely, the EPOS models include a hydrodynamic-like core and string-fragmentation dynamics, which increase the p_T of some produced Λ baryons and shift the yield toward higher p_T. Another contribution in this case is resonance feed-down from heavier strange baryons (*e.g.* $\Sigma^* \to \Lambda + \pi$), which slightly broadens the spectrum. The late hadronic stage is not necessarily the same in SMASH and EPOS and this is something that could be responsible for the harder Λ spectra in EPOS. The EPOS predictions at 6 GeV already indicate the onset of nontrivial collective or string-like effects compared to AGS and SPS systematics, with most Λ spectra remaining soft and exponential. NICA Λ p_T measurements will therefore provide an important initial test of whether strangeness in a baryon-rich regime is collectively hardened.

The p_T spectrum of π^+ at 7 GeV is shown in Fig. 5(a). The same pattern is observed at 7 GeV, except that all spectra are slightly hardened (flattened): EPOS-LHC and EPOS-4 are flatter than SMASH in the intermediate-p_T window, and the absolute yields are higher. The physical explanation is that small increases in available energy allow more secondary scatterings and slightly stronger collective effects in the EPOS models, modestly shifting the yield to higher p_T. In SMASH, hadronic rescattering is the dominant mechanism, and without an explicit early dense medium it cannot produce the intermediate-p_T tail seen in EPOS. This panel thus demonstrates that the model separation remains strong under modest changes in energy. In practice, the NICA energy scan must be able to trace this evolution and determine whether hardening with $\sqrt{s_{NN}}$ is consistent with EPOS-like processes or with hadronic transport.

The p_T spectrum of π^- at 7 GeV is shown in Fig. 5(b). The π^+ observations are confirmed by the π^- distribution at 7 GeV: the EPOS models predict a more pronounced intermediate-p_T component compared to SMASH. Physically, this indicates that processes responsible for transverse-momentum transfer, such as hydrodynamic pressure gradients in a core, more energetic string fragmentation, or multiple low-angle scatterings, are more effective in EPOS. Minor variations between EPOS-LHC and EPOS-4 are related to implementation and tuning choices (core fraction, string tension, viscous damping), but both clearly differ from SMASH. This panel further supports the view that the intermediate-p_T region should be a focus of the initial NICA analyses.

In the K^+ spectrum at 7 GeV, shown in Fig. 5(d), the yield increases relative to 6 GeV because associated production becomes more frequent at the higher energy. EPOS-4 still predicts a higher normalization and a flatter, harder spectrum than SMASH, with EPOS-LHC again intermediate. This difference arises because kaons are much less affected by resonance decays than pions; their slopes depend strongly on the dynamics of their production. In EPOS-4, the increased production channels and radial acceleration lead to flatter and more extended distributions. In SMASH, kaons are confined to near-

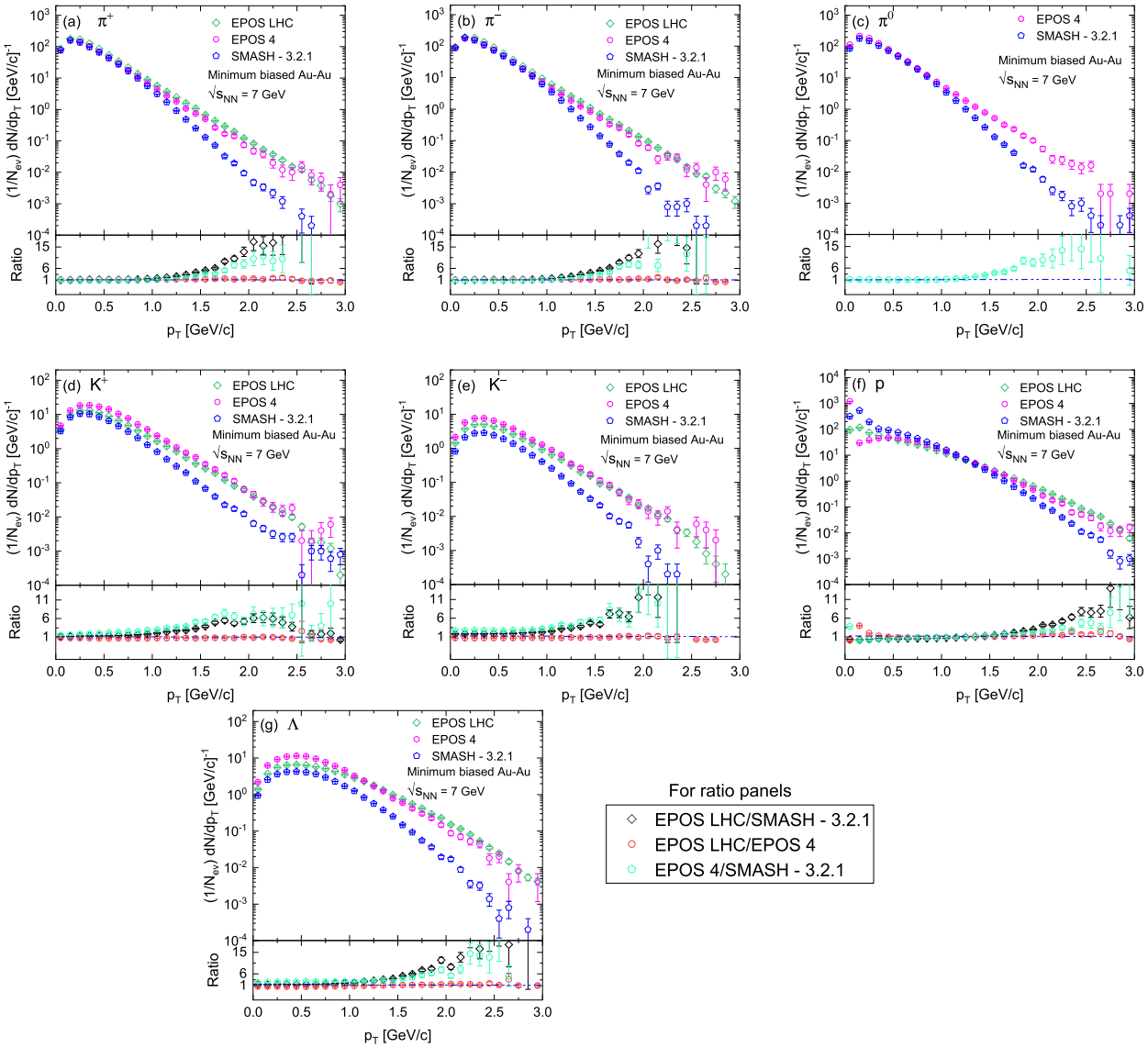


Fig. 5. (color online) Event-normalized $\mathrm{d}N/\mathrm{d}p_T$ transverse-momentum spectra of identified hadrons in minimum-bias Au + Au collisions at $\sqrt{s_{NN}} = 7$ GeV. The EPOS-LHC, EPOS-4, and SMASH model predictions are compared to demonstrate variations in the shape of the spectrum, slope (soft vs. hard components), and relative yield at low and intermediate p_T.

threshold hadronic production, resulting in steeper spectra. Physically, this makes kaons clean probes of strangeness production and flow. From the literature, kaon slopes were already known to be important for diagnosing collectivity at SPS [40, 11]. What is new here is that even at the 7 GeV scale, kaons are highly model dependent, implying that they will be decisive in future NICA measurements.

Figure 5(e) represents the K^- p_T distributions at 7 GeV. The increase in K^- spectra at 7 GeV contrasts with the lower yields at 6 GeV, but the overall production remains suppressed, with SMASH predicting the steepest slope and lowest yields. EPOS-4, on the other hand, yields higher multiplicities and less skewed distributions, with more efficient $s\bar{s}$ pair production. The physical explanation is that the hadronic thresholds in SMASH do not easily permit K^- production, whereas the string dynamics of EPOS-4 allow it. The harder, more slowly falling EPOS-4 spectrum is consistent with greater transverse-momentum transfer to the produced pairs than in SMASH. The importance of this observable is that K^- production directly tests whether pair creation is confined to hadronic scatterings. Based on the literature, K^- spectra played a significant role at SPS in identifying non-hadronic behavior [40]. The novelty here is that K^- at 7 GeV already shows such deviations in the model predictions, making it a particularly sensitive probe for NICA.

In SMASH and EPOS-4, protons at 7 GeV show increased normalization, as shown in Fig. 5(f), but they re-

tain the steep and flatter slope patterns, respectively. The physical explanation is that in SMASH, protons freeze out mostly via hadronic scatterings with little radial flow. In contrast, in EPOS-4, hydrodynamic-like expansion increases proton yields more effectively, resulting in more complex spectra. EPOS-LHC is again intermediate, as it includes hybrid physics. This is important because protons provide direct information on baryon transport and collectivity, and their spectral slopes can clearly distinguish hadronic from hybrid models. More generally, radial-flow sensitivity was also found to affect baryon slopes at RHIC BES [15], and these findings are now extended to the 7 GeV scale. The novelty here is that proton spectra, even at these relatively low energies, can strongly discriminate between competing dynamics.

The Λ spectrum at 7 GeV is shown in Fig. 5(g). The hierarchy remains the same: SMASH gives the steepest distribution, while EPOS-LHC and EPOS-4 are flatter, with EPOS-LHC slightly harder. The total yield is larger than at 6 GeV because of the greater phase space for strange-baryon production. The energy dependence is subtle but systematic, and the increasing intermediate-p_T yield in EPOS relative to SMASH indicates the growing role of collective-like dynamics in hybrid models. Physically, Λ baryons are produced both directly and through feed-down from higher-mass states. At 7 GeV, feed-down includes Σ and Ξ, and the transverse impulse in EPOS is stronger, so even secondary Λ baryons receive more momentum than in SMASH. The Λ spectra can also be influenced by the treatment of the late hadronic stage: rescattering can change the momentum of secondary Λ baryons, and the different prescriptions used for the core-corona and hadronic-evolution determine the amount of transverse momentum retained. These measurements are related to those from the SPS era [48], where Λ hardening was used as an indicator of collective expansion; the simulations show that similar behavior could also be observed at NICA energies. Fig. 5(g) suggests that differences in Λ slopes in the intermediate-p_T region are pronounced and could distinguish hadronic from core-corona dynamics.

Figure 6(a) shows the p_T distribution of π^+ at 8 GeV. Once again, the intermediate-p_T hardening in EPOS-LHC and EPOS-4 relative to SMASH is somewhat stronger than at lower energies. EPOS-LHC is slightly flatter than EPOS-4, but both show higher yields in the intermediate-p_T range than SMASH. The physical origin is the same: the effective core and string dynamics of EPOS generate a larger fraction of pions with higher transverse momentum, whereas the hadronic cascade in SMASH does not. The increase in energy enhances the visibility of this behavior, since more energy per nucleon leads to greater conversion into transverse energy. Experimentally, this panel shows that any energy-dependent hardening in the π^+ spectrum would be a critical discriminator: an EPOS-like trend would suggest increasing collective or semi-hard contributions with energy.

The same conclusions follow from the π^- p_T spectrum at 8 GeV, as shown in Fig. 6(b): the EPOS models continue to exhibit flatter intermediate-p_T slopes than SMASH, and the relative differences remain unchanged or vary only slightly with energy. Since charged-pion spectra are among the most precise data available experimentally, these panels provide a practical route for constraining the existence and strength of collective-like transverse dynamics at NICA energies. Combined with baryon and strangeness observables, the π^+ and π^- distributions provide a comprehensive picture of the initial and final stages of the collision.

The best separation of models is observed at 8 GeV in the K^+ spectra, as shown in Fig. 6(d). EPOS-4 yields higher multiplicities and much flatter slopes, whereas SMASH is markedly steeper. The physical explanation is that associated-production channels are more common at this energy, and the string dynamics of EPOS-4 enhance both yield and flow. In SMASH, kaons are confined to hadronic scattering and are therefore more limited in their spectra. What is important is that kaons provide a direct measure of strangeness enhancement and collective dynamics, and their slopes at 8 GeV are strongly model dependent. This observable may offer the cleanest test of competing models at NICA.

The increase in K^- yields continues at 8 GeV, as displayed in Fig. 6(e), but suppression relative to K^+ remains. EPOS-4 generates larger yields and flatter slopes, while the SMASH yields are steep and suppressed. The physical cause is that pair creation becomes more effective at higher collision energies; in models that allow string dynamics, this process occurs at the required rate. The importance is that K^- spectra can serve as a clear identifier of hadronic-only versus hybrid approaches. More generally, the argument for nonhadronic dynamics was based on the slope of K^- at SPS, and we have applied the same logic at 8 GeV. The difference is that K^- spectra at NICA energies can more clearly determine whether partonic-like processes are already present.

Proton p_T spectra at 8 GeV, given in Fig. 6(f), again show steeper slopes in SMASH than in EPOS-4 and EPOS-LHC. The physical cause is that collective radial expansion is stronger at higher collision energies in the EPOS framework, which shifts protons to higher p_T. Protons in SMASH are limited to hadronic scatterings, which produce softer slopes. The importance is that protons carry baryon number and directly probe stopping and radial flow, and the models clearly distinguish their slopes. In the literature, baryon slopes at RHIC BES were considered key to diagnosing the emergence of collectivity [15], and our results show the same sensitivity in the NICA range. The new aspect here is that proton slopes at 8 GeV can be among the clearest discriminators between

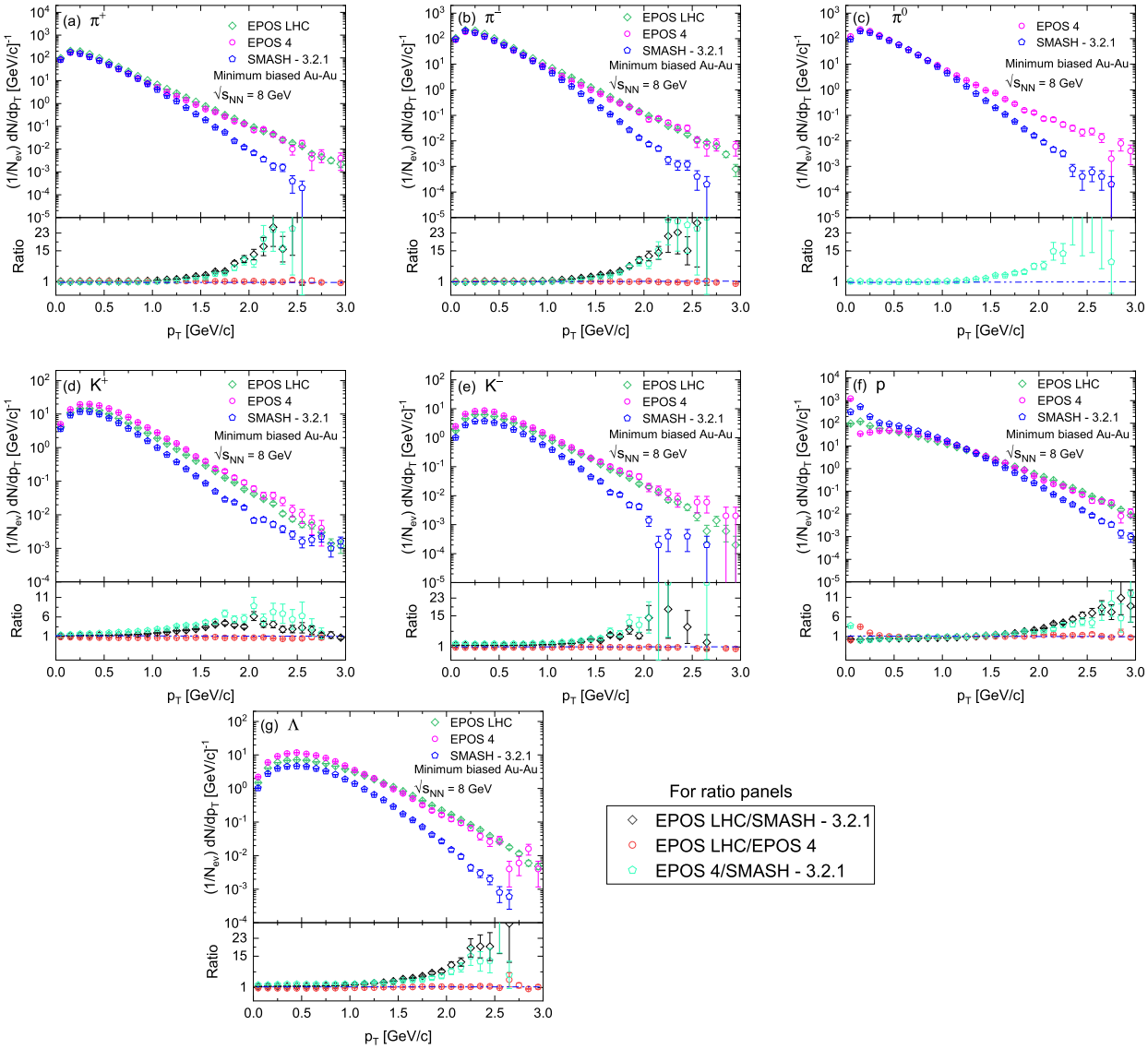


Fig. 6. (color online) Transverse-momentum spectra (event-normalized $\mathrm{d}N/\mathrm{d}p_T$) of identified hadrons in minimum-bias Au + Au collisions at $\sqrt{s_{NN}} = 8$ GeV.

hadronic and partonic processes.

The spectrum of the Λ is shown in Fig. 6(g) at $\sqrt{s_{NN}} = 8$ GeV. The results separate most clearly into SMASH, EPOS-4, and EPOS-LHC. SMASH is the only model that produces a steep slope, while EPOS-4 and, more so, EPOS-LHC yield very flat spectra, retaining substantial yield in the $0.8-3$ GeV/c region [49]. The total Λ yield is again larger, consistent with the increased energy available for strange-baryon production. Significantly, the EPOS curves develop a pronounced shoulder in the intermediate-p_T range that is absent in SMASH, reflecting the combined effects of stronger string excitations and collective transverse expansion at this energy. Physically, this pattern persists across $6-8$ GeV and therefore suggests that Λ spectra are sensitive to transverse-expansion dynamics and freeze-out, as well as strangeness production. Feed-down contributions still exist, but in EPOS the hard momentum distribution of the parent states is inherited by feed-down Λ baryons, whereas in SMASH the late-stage hadronic feed-down remains mostly soft. The EPOS results at 8 GeV indicate that NICA may be able to identify collective-like spectral behavior at lower energies than previously suggested, owing to the energy-dependent hardening of the Λ spectra in the present minimum-bias samples. Experimentally establishing such hardening would provide evidence for stronger transverse-momentum generation affecting strange baryons, although a combined comparison of several observables would be required to determine its microscopic origin.

C. $p_T - y$ mapping

The purpose of the two-dimensional $p_T - y$ maps is to show where longitudinal particle production and transverse-momentum generation occur simultaneously, rather than merely to reproduce the separate one-dimensional distributions. For K^-, the populated rapidity width and transverse-momentum extent are sensitive to the model-dependent balance among strange-pair production, strangeness-exchange processes, absorption, and subsequent rescattering in baryon-rich matter. For Λ, the maps combine sensitivity to associated strangeness production, strange-baryon transport, resonance feed-down, and transverse spectral broadening. Their principal role in the present study is to identify the phase-space regions in which future higher-statistics MPD/NICA measurements can most effectively distinguish among the model predictions.

The rare-particle maps must nevertheless be interpreted within their statistical limitations. No quantitative conclusion is drawn from isolated outer cells or from regions in which the K^- or Λ distributions are sparsely populated. Model comparisons are restricted to the continuous, populated region around midrapidity and low-to-intermediate p_T.

Figures 7(a-c) show the π^+ 2D $p_T - y$ distributions at 6 GeV in EPOS-LHC, EPOS-4, and SMASH, respectively, and Figs. 7(d-f) show the π^- distributions. In all cases, the yield is strongly concentrated at low transverse momenta ($p_T < 0.8\,\mathrm{GeV}/c$) and forms a bright band at midrapidity. The magnitude also decreases gradually with increasing y and p_T. EPOS-LHC and EPOS-4 show somewhat more extended p_T distributions at midrapidity ($y \approx 0$) and still retain yield up to approximately $1.5\,\mathrm{GeV}/c$, whereas SMASH is slightly more confined to the soft sector. The rapidity profiles are all symmetric and centered at $y \approx 0$. The same overall features are found at $\sqrt{s_{NN}} = 7$ GeV (Figs. 8(a-f)), with a stronger intermediate-p_T enhancement in the EPOS models. EPOS-LHC still maintains visible yield up to a maximum of $1.8\,\mathrm{GeV}/c$, while SMASH remains focused on p_T below $1.3\,\mathrm{GeV}/c$. At $\sqrt{s_{NN}} = 8$ GeV (Figs. 9(a-f)), the contrast increases slightly: the EPOS models exhibit non-negligible population up to a few GeV/c, whereas SMASH remains steep and concentrated at lower transverse momenta. The rapidity distributions are largely universal across models at all energies. These maps demonstrate that pion production at this energy scale is dominated by resonance decay (*e.g.*, $\Delta \to N\pi$, $\rho \to \pi\pi$) and soft hadronic reactions. The small differences between models arise because the string and core dynamics in EPOS provide a modest, but systematic, enhancement in the intermediate p_T region. Charged pions are therefore a robust baseline observable that is sensitive to multiplicity normalization but exhibits limited discriminating power between hadronic and hybrid descriptions.

The K^+ distributions are presented in Figs. 7(g-i), and the K^- distributions in Figs. 7(j-l), at $\sqrt{s_{NN}} = 6$ GeV. For K^+, the maps extend farther in p_T than those for pions, reaching up to about $1.5\,\mathrm{GeV}/c$, and the p_T spectra and rapidity coverage of EPOS-LHC and EPOS-4 are broader than those in SMASH, where they are steeply confined below $1.1\,\mathrm{GeV}/c$ and are narrower around $y \approx 0$. For K^-, pair-production channels are strongly reduced and are suppressed in baryon-rich systems; the same hierarchy therefore applies, with the EPOS models showing broader p_T tails and slightly wider rapidity distributions. At 7 GeV (Figs. 8(g-l)), the kaon yields increase, and the EPOS models exhibit stronger populations in the intermediate-p_T region, whereas SMASH remains steep and localized. The rapidity range also extends slightly in the EPOS models, especially for K^+. The separation is most apparent at 8 GeV (Figs. 9(g-l)): EPOS-LHC retains substantial yield up to approximately $2\,\mathrm{GeV}/c$ and shows visibly more extensive rapidity coverage, whereas the SMASH distributions remain thin and weak. This physically reflects the interplay of the mechanisms governing strangeness production. The production of K^+ is dominant because the associated processes ($NN \to N\Lambda K^+$) are enhanced in baryon-rich collisions at the expense of K^- production. EPOS models also provide additional transverse momentum through string excitation and early collective effects, whereas SMASH generates momentum through late hadronic rescattering. The kaon $p_T - y$ maps are therefore sensitive probes of strangeness dynamics and early-stage collectivity, and model variations become apparent in the intermediate-p_T region and in the K^+/K^- asymmetry.

Figures 7(m-r) present the proton and Λ $p_T - y$ distributions at $\sqrt{s_{NN}} = 6$ GeV, respectively for EPOS-LHC, EPOS-4, and SMASH. There is a clear difference among the models. SMASH shows the steepest falloff in transverse momentum: most protons are concentrated below $p_T \approx 1\,\mathrm{GeV}/c$. Nevertheless, SMASH has the widest rapidity coverage, with yields extending significantly toward forward and backward rapidities. In comparison, EPOS-LHC and EPOS-4 produce slightly flatter p_T spectra, with visible populations at higher transverse momenta (up to $2\,\mathrm{GeV}/c$). However, their rapidity distributions are more concentrated at midrapidity ($y \approx 0$), indicating stronger stopping. These differences become more pronounced at $\sqrt{s_{NN}} = 7$ GeV (Figs. 8(m-o)). SMASH is still characterized by broad rapidity distributions, with protons displaced further in y as energy increases, although the spectra remain steep in p_T. The EPOS models instead produce narrower rapidity peaks centered more closely around $y \approx 0$, but with harder transverse-momentum tails that extend into the intermediate-p_T regime ($1.5 - 3\,\mathrm{GeV}/c$). The separation is greatest at $\sqrt{s_{NN}} =$ 8 GeV (Figs. 9(m-o)). SMASH yields the broadest proton rapidity distribution among all models, yet confines

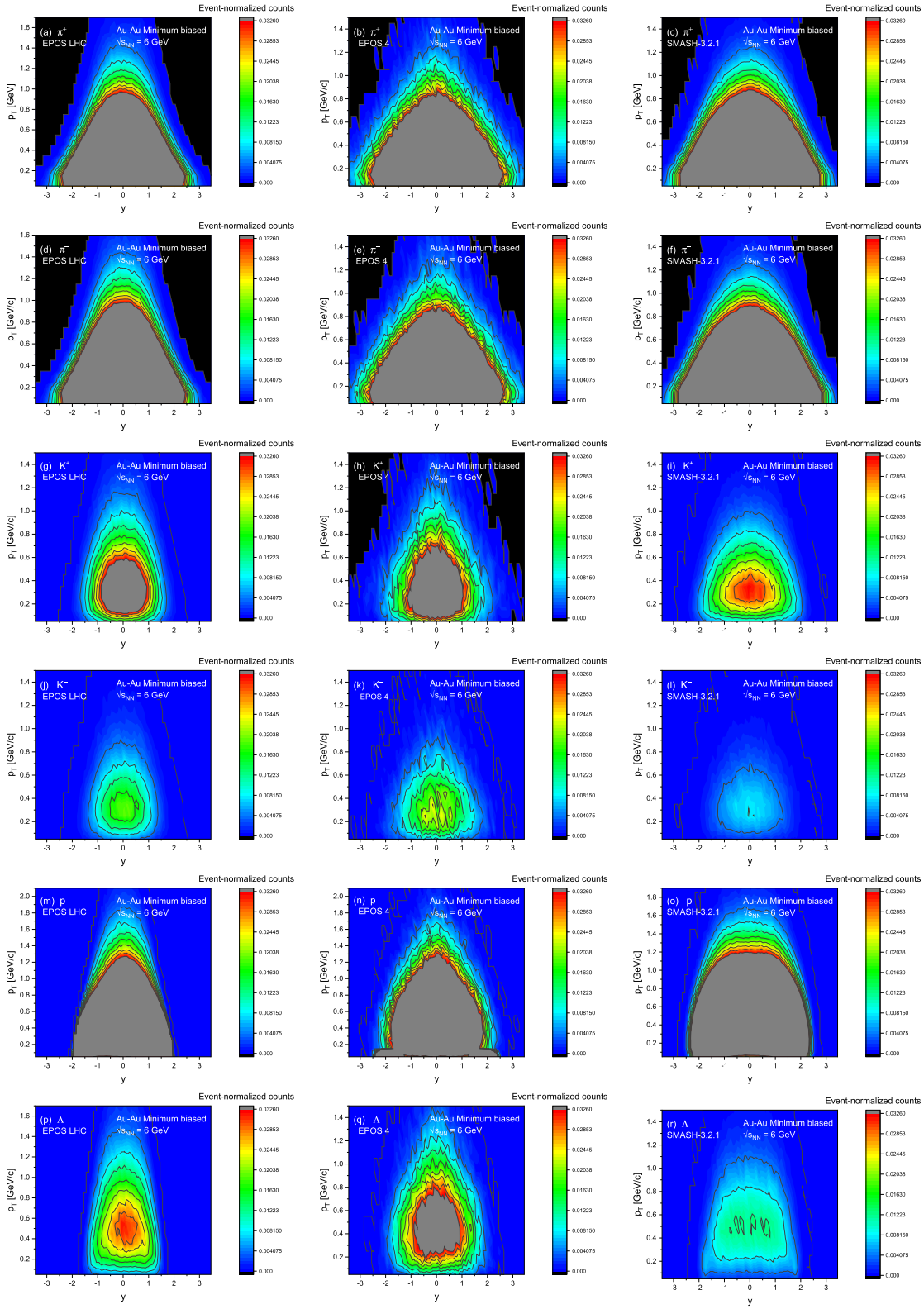


Fig. 7. (color online) Two-dimensional p_T vs rapidity density maps (color scale = event-normalized counts) of various identified hadrons in minimum-bias collision of Au + Au in $\sqrt{s_{NN}} = 6$ GeV. The arrangement of the panels is three columns (left-right: EPOS-LHC, EPOS-4, SMASH) and numerous rows (by species). Particularly: (a)-(c) π^+ (EPOS-LHC / EPOS-4 / SMASH), (d)-(f) π^-, (g)-(i) K^+, (j)-(l) K^-, (m)-(o) p and (p)-(r) Λ. The color scale indicates relative event-normalized population in the $p_T - y$ plane and points out variations in the manner each model populates intermediate p_T and non-central rapidities.

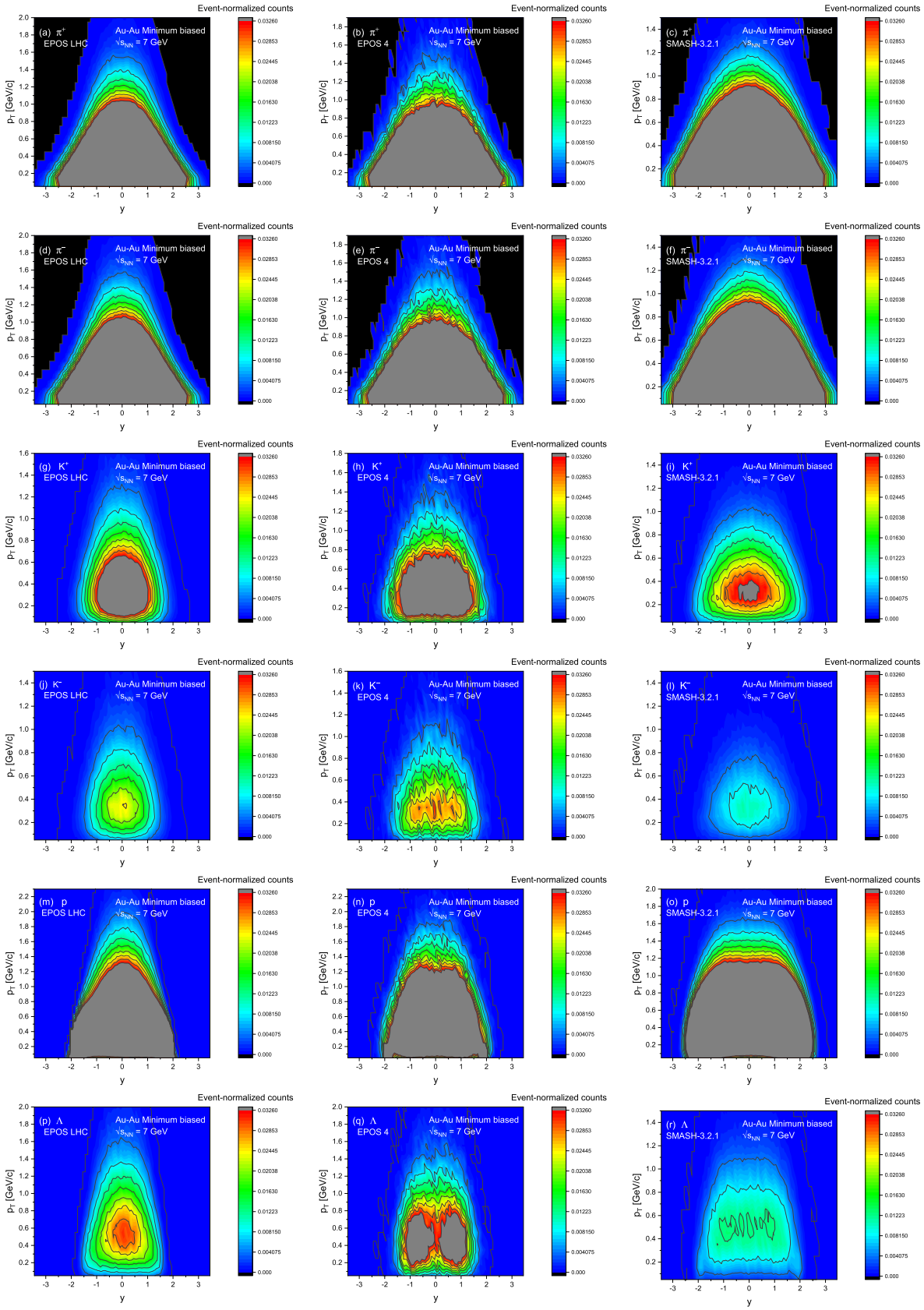


Fig. 8. (color online) Two-dimensional p_T vs rapidity density maps (color scale = event-normalized counts) of various identified hadrons in minimum-bias collision of Au + Au in $\sqrt{s_{NN}} = 7$ GeV. The arrangement of the panels is similar to Fig. 7.

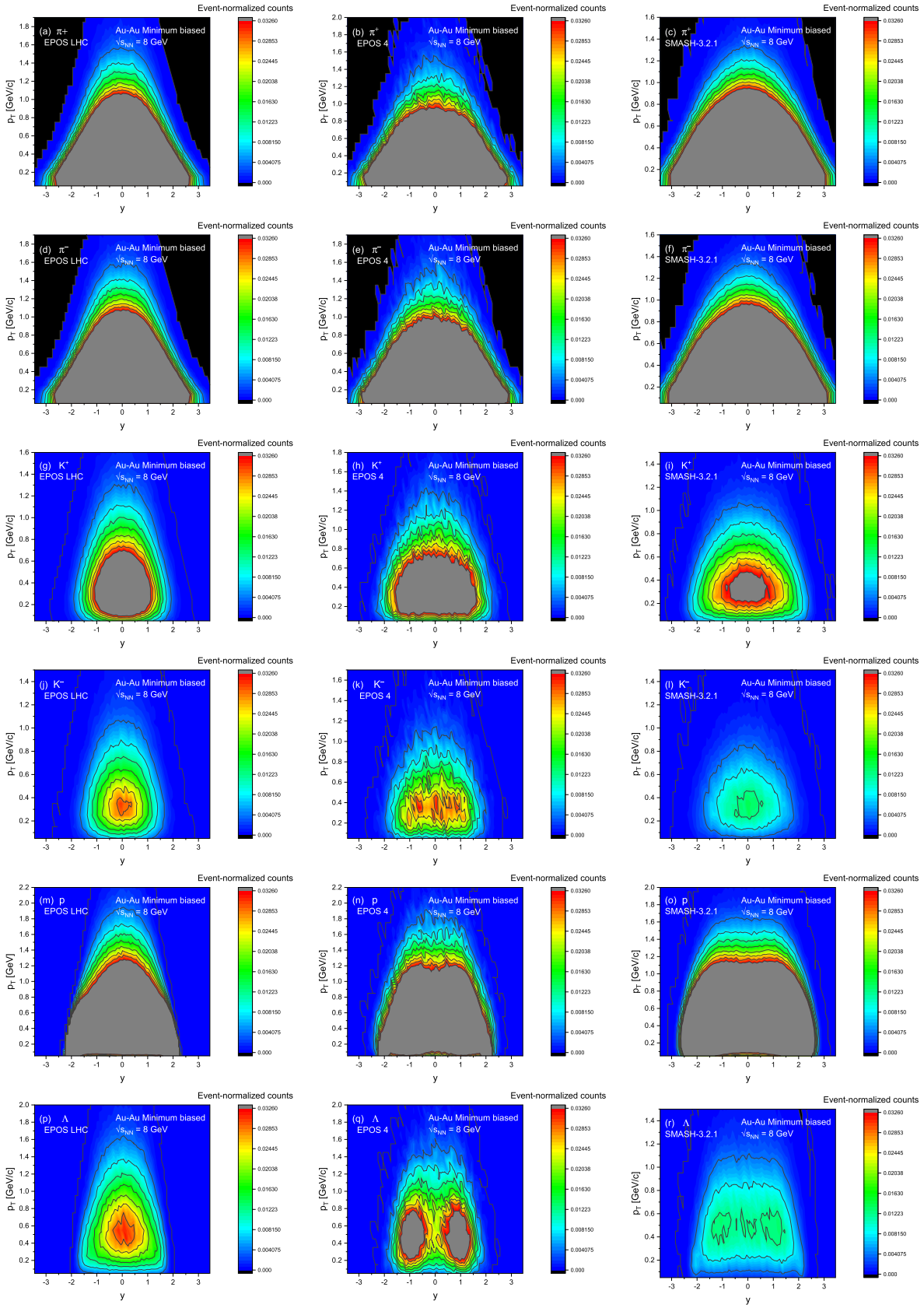


Fig. 9. (color online) Two-dimensional p_T vs rapidity density maps (color scale = event-normalized counts) of various identified hadrons in minimum-bias collision of Au + Au in $\sqrt{s_{NN}} = 8$ GeV. The arrangement of the panels is similar to Figs. 7 and 8.

protons to soft p_T ($< 1\,\mathrm{GeV}/c$). EPOS-LHC and EPOS-4 are narrower in rapidity, but have much harder transverse-momentum spectra, with substantial populations extending to $2-2.5\,\mathrm{GeV}/c$. These systematic discrepancies highlight the complementary nature of the models' physics. In SMASH, baryon transport is purely hadronically rescattered, which results in weaker stopping, a wider rapidity distribution, and weaker transverse acceleration. Owing to the incorporation of core-corona dynamics and string excitation, the EPOS models exhibit stronger stopping (smaller rapidity peaks) and a stronger transverse push (flatter p_T spectra) [26, 50]. In short, the hierarchy is as follows: rapidity coverage is wider in SMASH, whereas transverse-momentum hardness is stronger in EPOS. This twofold pattern is a useful discriminator. Stopping and collective expansion are encoded in protons, which are the main carriers of baryon number. The $p_T - y$ distributions therefore indicate whether the system evolves as a purely hadronic, strongly transported medium (SMASH) or exhibits stronger stopping and transverse dynamics (EPOS).

Figures 7(p-r) display the Λ $p_T - y$ distributions at $\sqrt{s_{NN}} = 6\,\mathrm{GeV}$. All models exhibit yields concentrated at low p_T around midrapidity; however, SMASH produces the sharpest and narrowest distributions. In contrast, EPOS-LHC and EPOS-4 have non-negligible populations extending up to about $1.5-2\,\mathrm{GeV}/c$ and cover a more extended rapidity range. The separation is more pronounced at 7 GeV (Figs. 8(p-r)), where the EPOS models form visible shoulders in the intermediate-p_T region at midrapidity that are absent in SMASH [26, 50, 32]. The difference is greatest at 8 GeV (Figs. 9(p-r)). The SMASH distributions are restricted to low p_T and $y \approx 0$, whereas EPOS-LHC and EPOS-4 show broader and flatter distributions with p_T up to about $2\,\mathrm{GeV}/c$ as well as larger rapidity coverage. This hierarchy arises because the treatment of strange-baryon production and freeze-out differs. In SMASH, Λ particles are produced through hadronic associated mechanisms ($NN \to N\Lambda K$) and subsequently rescatter extensively, resulting in a soft and centrally peaked distribution. The EPOS models can include early string excitation and core-corona dynamics, giving rise to harder parent states (Σ^*, Ξ) whose decays feed down to harder Λ states and which freeze out earlier with a stronger transverse push. Consequently, the EPOS models predict Λ distributions that are harder in p_T and broader in rapidity. Λ baryons are the most sensitive probes of the underlying dynamics among all species investigated. They are sensitive to collective expansion because of their larger mass and their strong coupling to the medium. If the future NICA measurements give flatter and broader Λ distributions as predicted by EPOS, then this would support descriptions with stronger collective transverse dynamics. This observable is not sufficient to determine the microscopic origin of the broadening though, and several observables would be needed to make this determination. On the other hand, if SMASH-like patterns are observed, an all-hadronic evolution picture would be preferred.

D. NCQ-scaled elliptic flow

Anisotropic flow coefficients were computed with an event-plane–type estimator using Q-vectors constructed from all final-state particles with p_T weights. For each harmonic n—although only $n = 2$ is used in the present manuscript—the event-plane angle was defined from the event flow vector (Q-vector) [51]:

$$Q_n = \sum_j w_j \mathrm{e}^{\mathrm{i}n\phi_j}. \tag{2}$$

The sum runs over the j particles used in the event-plane determination, w_j is the weight, defined as $w_j = p_{T,j}$, and ϕ is the azimuthal angle of the particle's transverse momentum around the beam direction. Eq. (2) implies

$$\begin{aligned} Q_{n,x} &= \sum_j w_j \cos(n\phi_j) \text{ and} \\ Q_{n,y} &= \sum_j w_j \sin(n\phi_j). \end{aligned} \tag{3}$$

The event-plane angle is then defined as

$$\Psi_n = \frac{1}{n} \mathrm{atan2}\left(Q_{n,y}, Q_{n,x}\right). \tag{4}$$

Differential flow is accumulated in p_T bins as follows:

$$v_n(p_T) = \langle \cos\left[n\left(\phi - \Psi_n\right)\right] \rangle_{p_T \text{ bin}}, \tag{5}$$

averaged over particles in a single event or collision.

No η gap, subevent method, or event-plane-resolution correction was applied in the present implementation. The same generator-level estimator was used for all three models to provide a common baseline for comparison; accordingly, the resulting coefficients are not presented as detector-level, resolution-corrected flow measurements.

Figure 10 presents the elliptic-flow coefficient divided by the number of constituent quarks, v_2/n_q, as a function of the transverse kinetic energy per constituent quark,

$$\frac{KE_T}{n_q} = \frac{m_T - m_0}{n_q} = \frac{\sqrt{p_T^2 + m_0^2} - m_0}{n_q}, \tag{6}$$

where m_0 is the hadron rest mass. We use $n_q = 2$ for

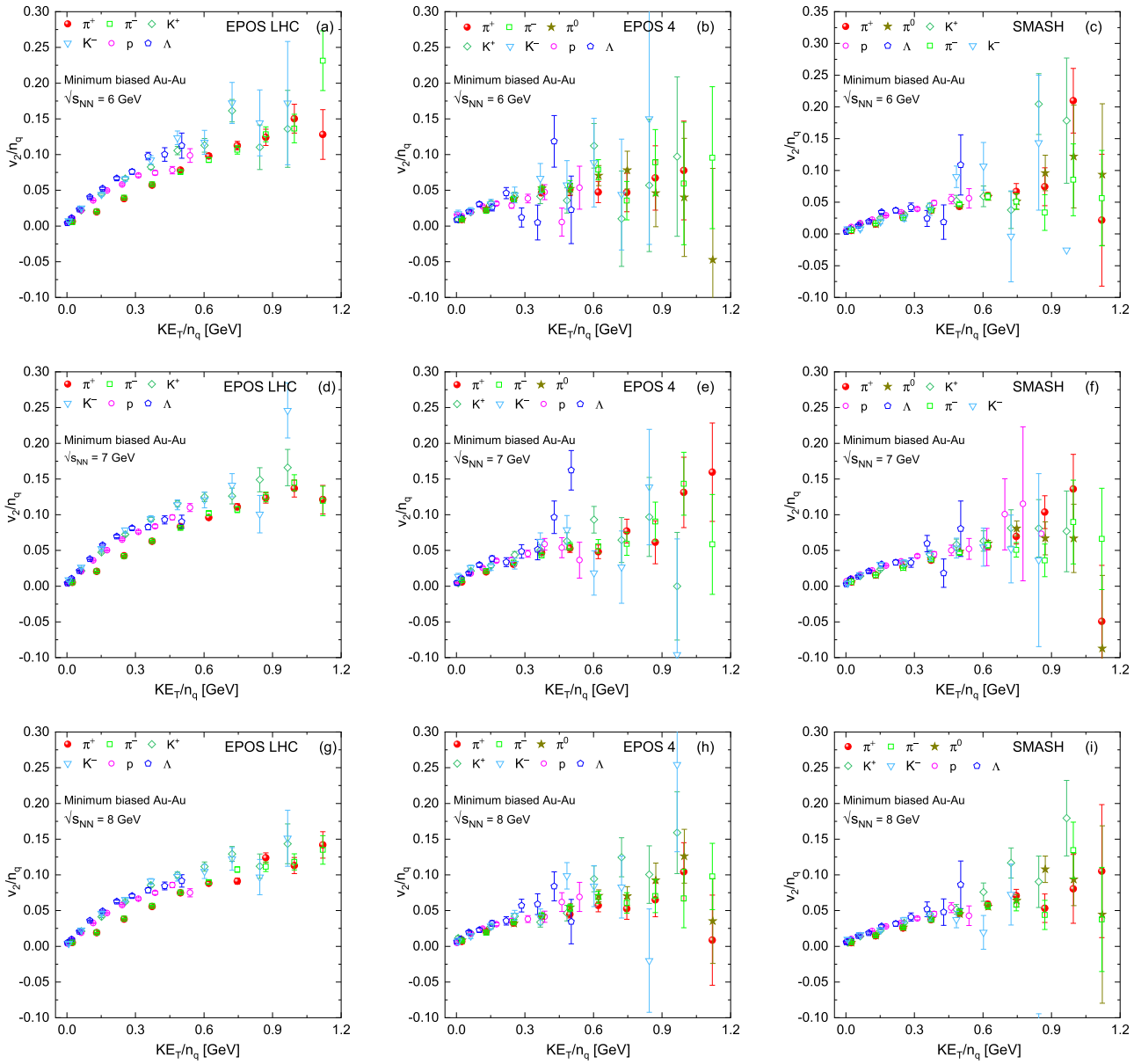


Fig. 10. (color online) Number-of-constituent-quark-scaled elliptic flow, v_2/n_q, as a function of transverse kinetic energy per constituent quark, KE_T/n_q, for identified hadrons in minimum-bias Au+Au collisions at $\sqrt{s_{NN}} = 6$, 7, and 8 GeV. Mesons use $n_q = 2$ and baryons use $n_q = 3$. EPOS-LHC provides the closest approximate visual grouping in the statistically populated region, while EPOS-4 and SMASH show larger species-dependent deviations. The highest-KE_T/n_q points are not used for quantitative conclusions because of their large statistical uncertainties. Neutral pions are shown for EPOS-4 and SMASH as consistency observables; the public EPOS-LHC output used here does not provide an equivalent direct π^0 comparison.

mesons and $n_q = 3$ for baryons. The KE_T/n_q representation reduces the kinematic effect of hadron-mass ordering relative to p_T/n_q and is commonly used to test approximate constituent-quark scaling.

In the statistically populated low- and intermediate-KE_T/n_q region, the common particle species in all three models exhibit an approximately increasing trend. Among the three calculations, EPOS-LHC shows the closest visual grouping of mesons and baryons at $\sqrt{s_{NN}} = 6$, 7, and 8 GeV. Its charged pions, kaons, protons, and Λ baryons remain within a comparatively narrow common band over most of the populated interval. EPOS-4 and SMASH also show partial scaling, but they exhibit larger species-dependent deviations and stronger fluctuations at intermediate and high KE_T/n_q.

The collapse is not exact in any model. In EPOS-LHC, strange mesons and Λ baryons remain above the charged-pion trend in parts of the intermediate-KE_T/n_q interval, while the highest-KE_T/n_q points have large statistical uncertainties. The apparent hierarchy is therefore

confined to the statistically populated region and should be regarded as a visual comparison rather than a quantitative test of universal scaling.

The present v_2 calculation uses a common generator-level event-plane estimator for all three models. No detector-level acceptance, pseudorapidity gap, subevent separation, or event-plane-resolution correction is applied. Consequently, the comparison indicates how closely the three generator outputs approach a common scaled trend under an identical analysis prescription, but it should not be interpreted as direct evidence for a partonic phase, quark coalescence, or deconfinement.

E. Hadron ratios

The π^-/π^+ ratio as a function of p_T, shown in panels (a) of Figs. 11−13, is close to unity at all investigated energies and in all three models. This reflects the stability of pion production, since resonance decays maintain the isospin balance. The neutron excess in Au+Au collisions would, in principle, lead to a slight enhancement of π^- over π^+, but this effect is negligible and further diluted in the central rapidity region. This approximate symmetry is reproduced in both the SMASH and EPOS frameworks, indicating that isospin conservation is consistently respected in both. The absence of model dependence can be attributed to the fact that the resonance spectrum is the same in all frameworks, and its impact on pion yields is much larger than that of the other microscopic differences. Physically, this ratio serves as a cross-check rather than a diagnostic, since it tests only the most basic treat-

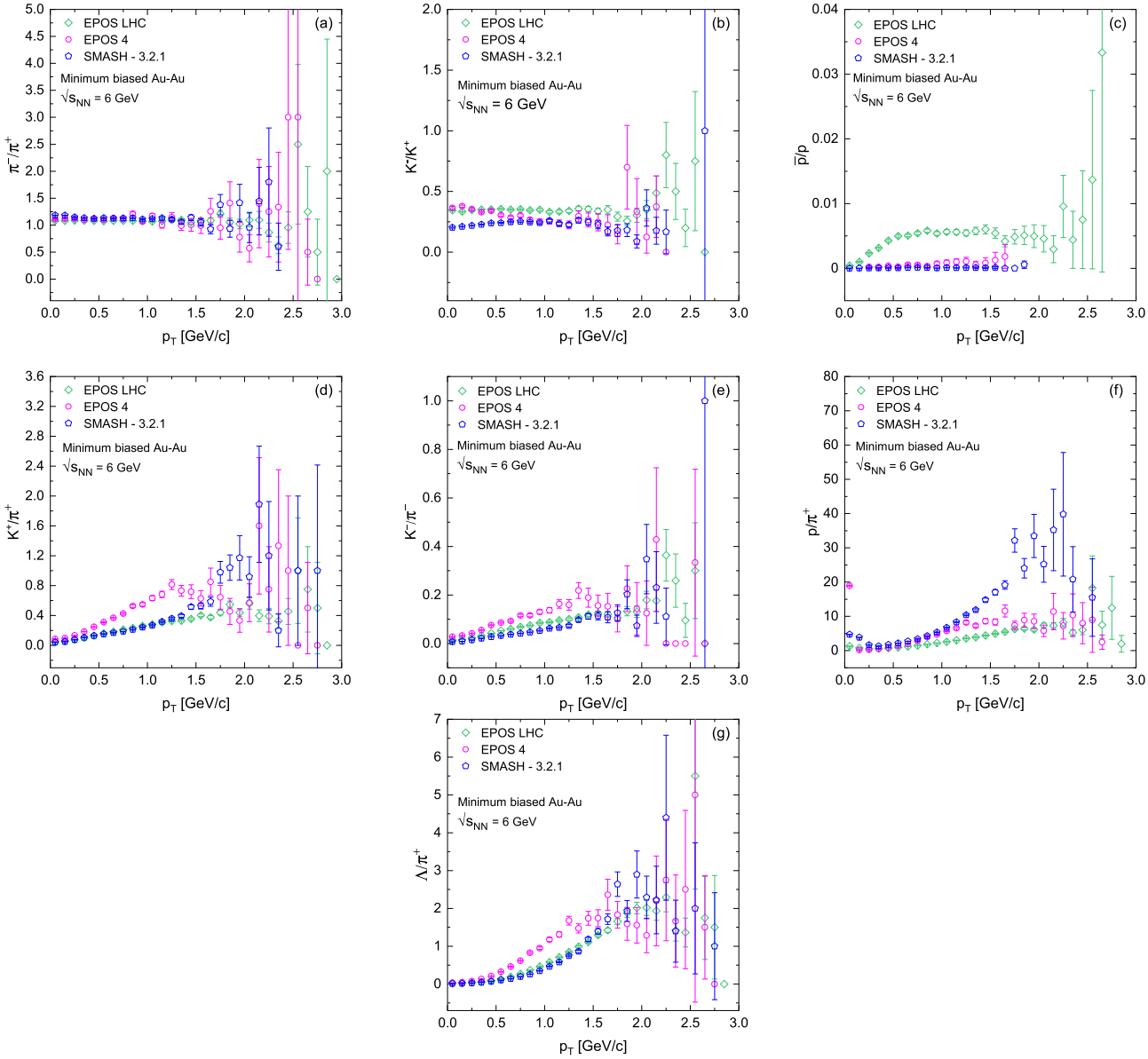


Fig. 11. (color online) Ratios of particle yields versus transverse momentum of minimum-bias Au + Au collisions at $\sqrt{s_{NN}} = 6$ GeV.

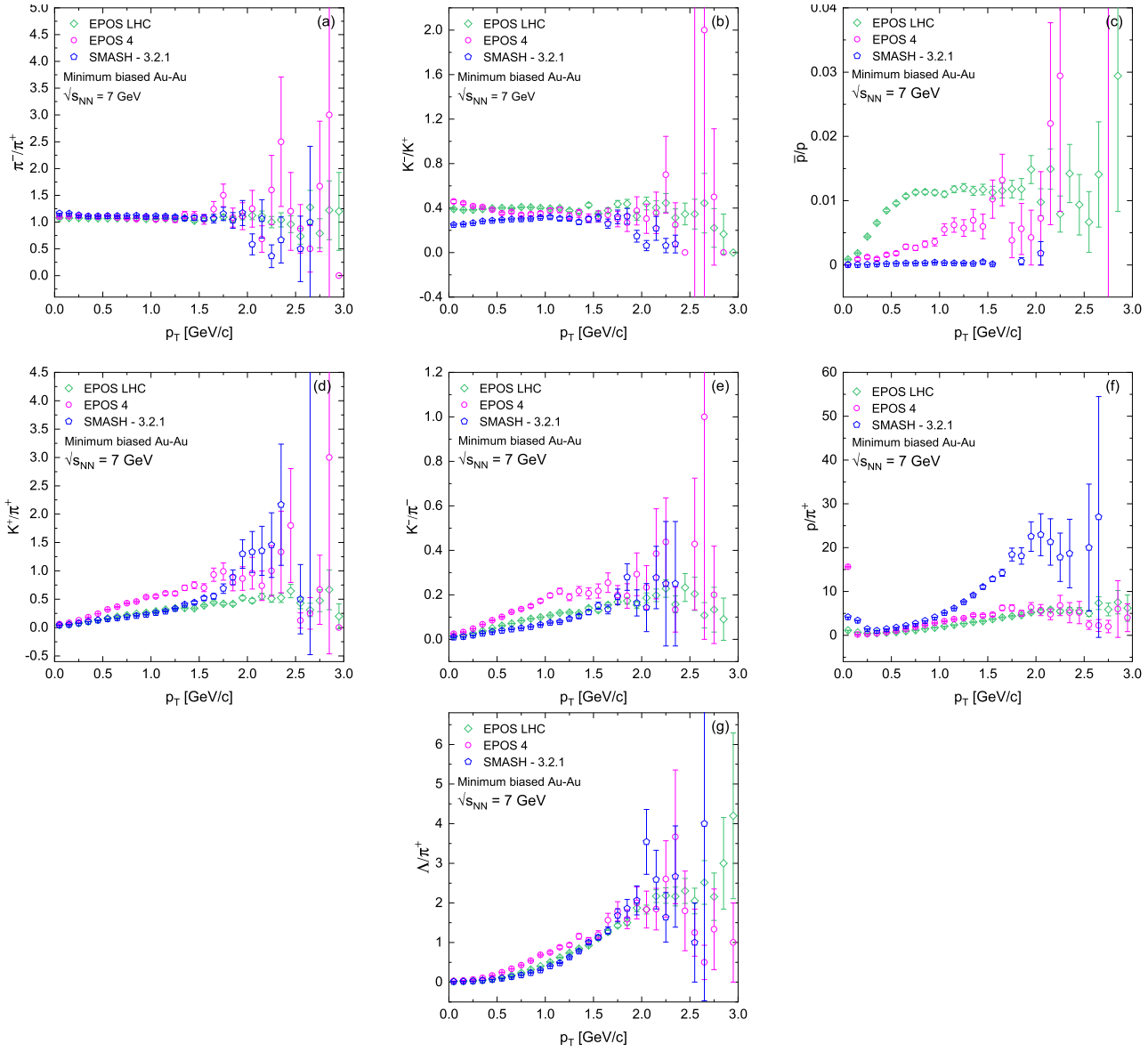


Fig. 12. (color online) Ratios of particle yields versus transverse momentum of minimum-bias Au + Au collisions at $\sqrt{s_{NN}} = 7$ GeV.

ment of isospin and not the internal dynamics. Nevertheless, its importance should not be underestimated: a constant π^-/π^+ ratio gives confidence that any deviations observed in more complex ratios (involving strangeness or baryons) arise from genuine dynamical effects, rather than trivial isospin effects. The novelty here is that this stability is explicitly confirmed in the previously unexplored 6−8 GeV regime, providing a firm basis for interpreting the more sensitive ratios.

The K^-/K^+ ratio (panels (b) of Figs. 11−13) is strongly suppressed (well below unity) across p_T at 6 GeV in all models, due to the dominance of associated K^+ production ($NN \to N\Lambda K^+$) and the energetic cost of producing K^- through $s\bar{s}$ pair production. At 7 and 8 GeV, this ratio generally increases, especially at intermediate p_T, but it remains typically below 1 in all models. EPOS-LHC and EPOS-4 predict a more pronounced increase in K^-/K^+ at intermediate p_T than SMASH; the EPOS codes place more yield in the hard kaon tail because string fragmentation and any core component transfer more transverse momentum to strange mesons. As a hadronic transport model, SMASH exhibits stronger low-p_T suppression of K^- and a steeper rise with p_T where K^- are produced. Physically, these variations probe the efficiency of pair production and in-medium K^- absorption. EPOS is more effective than SMASH in enhancing early pair production and reducing absorption. For NICA, a direct measurement of K^-/K^+ as a function of p_T will place strong constraints on strangeness pair-production and absorption models in a baryon-rich medium.

The $\bar{p}/p$ ratio is strongly suppressed at all three collision energies and shows clear model and energy depend-

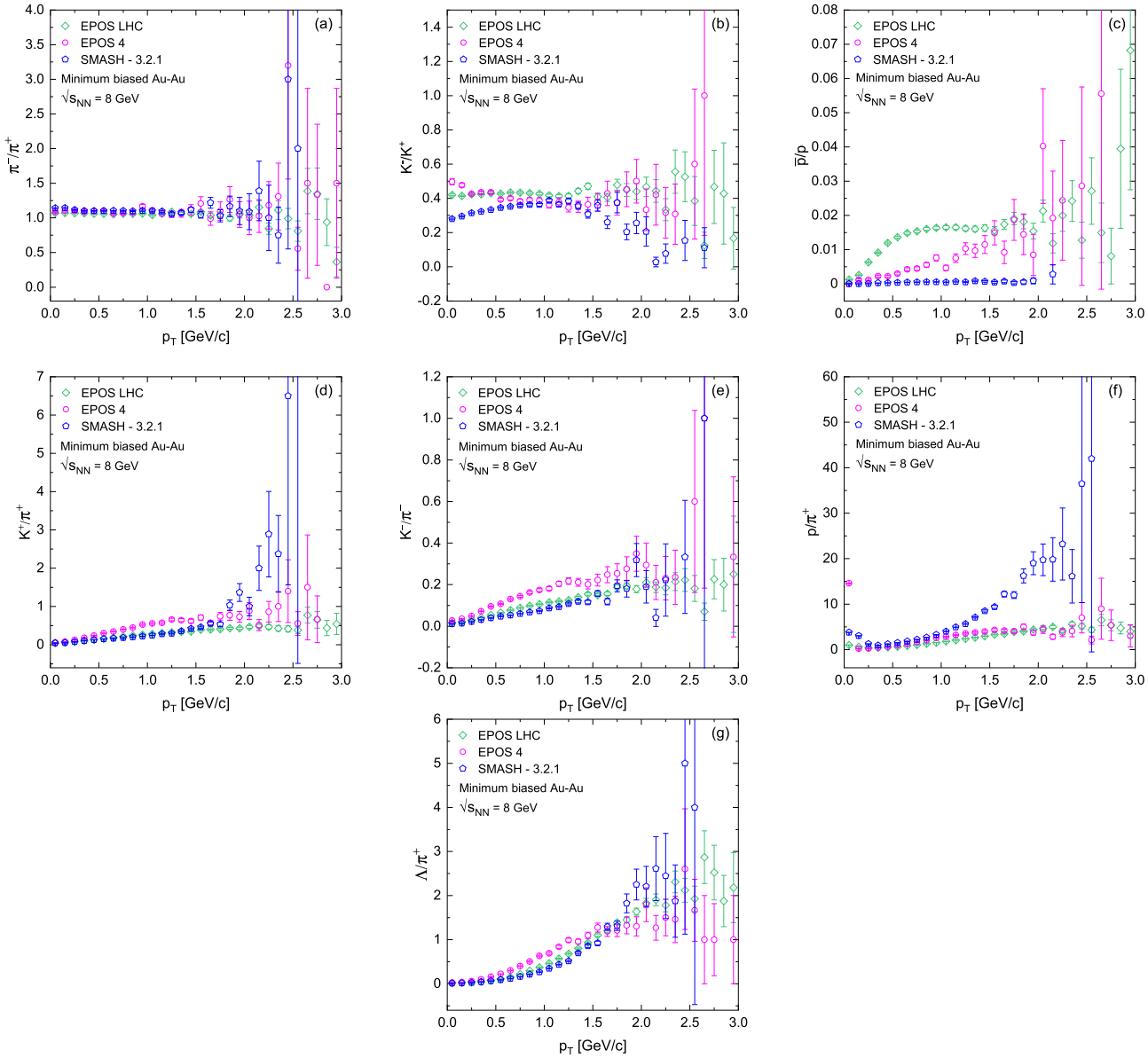


Fig. 13. (color online) Ratios of particle yields versus transverse momentum of minimum-bias Au + Au collisions at $\sqrt{s_{NN}} = 8$ GeV.

ence, as seen in panels (c) of Figs. 11–13. The ratio is not identically zero, as can be verified by direct inspection of the numerical SMASH-3.2.1 results. For $p_{\mathrm{T}} < 2.0\,\mathrm{GeV}/c$, the positive SMASH-3.2.1 values range approximately from 2.5×10^{-6} to 5.6×10^{-4} at $\sqrt{s_{NN}} = 6$ GeV, from 4.4×10^{-6} to 5.7×10^{-4} at $\sqrt{s_{NN}} = 7$ GeV, and from 9.5×10^{-6} to 8.8×10^{-4} at $\sqrt{s_{NN}} = 8$ GeV. These values are several orders of magnitude smaller than unity and therefore appear near the lower limit of the linear scale in the panels, sometimes seemingly zero. Bins for which no positive ratio is found are not used for quantitative interpretation.

To display the small positive values more clearly, Fig. 14 presents the same $\bar{p}/p$ results on a logarithmic vertical scale. The original linear-scale panels in Figs. 11–13 are retained to preserve a uniform presentation of all particle-yield ratios. In the statistically populated region, the SMASH-3.2.1 prediction for the antiproton fraction is generally smaller than those of EPOS-LHC and EPOS-4, as the logarithmic representation confirms. The pronounced model dependence of $\bar{p}/p$ reflects the different treatments of baryon–antibaryon production and annihilation in the three frameworks.

As a reference, the NA49 Collaboration measured a $\bar{p}/p$ ratio of about 10^{-3} for central Pb+Pb collisions at the lowest collision energy considered in Ref. [52] in the midrapidity region. This measurement is useful as an experimental reference scale, but a direct point-by-point comparison is not made. The NA49 result refers to central Pb+Pb collisions and a midrapidity, p_{T}-integrated

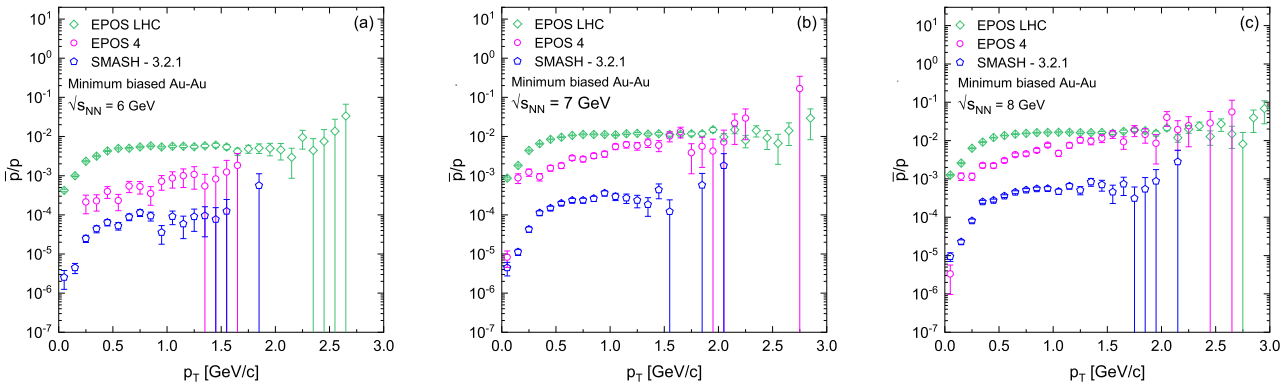


Fig. 14. (color online) The $\bar{p}/p$ ratio as a function of transverse momentum in minimum-bias Au+Au collisions at $\sqrt{s_{NN}} = 6$, 7, and 8 GeV, shown in panels (a), (b), and (c), respectively. The numbers shown in these panels are identical to those in panels (c) of Figures 11−13, but are shown here on a logarithmic vertical scale. The SMASH-3.2.1 values are so small that they are compressed visually into the lower panel boundary of the corresponding linear-scale panels, and the logarithmic representation is used to address this issue. There are only finite positive ratios shown; bins that have no finite positive ratio are not displayed on a logarithmic scale.

yield ratio, whereas the present results are minimum-bias, p_{T}-differential, generator-level Au+Au predictions without an additional rapidity selection.

The K^+/π^+ ratio (panels (d) of Figs. 11−13) increases with p_T at all energies; the increase is more pronounced as the collision energy rises from 6 to 8 GeV, consistent with Refs. [40, 53]. EPOS-4 systematically yields higher values of K^+/π^+ at intermediate p_T (0.8−3 GeV/c) than SMASH. Physically, the rise with p_T reflects the fact that heavier particles are kinematically favored at higher transverse momenta, and that kaon production relative to pion production in the intermediate region is enhanced by collective radial flow (or harder string fragments). The energy dependence (the increase from 6 to 8 GeV) is expected, since higher available energy leads to greater strangeness production and allows more semi-hard processes. The model differences therefore encode differences in the efficiency of producing and accelerating strange mesons: EPOS models convert more longitudinal energy into transverse momentum and/or generate more strangeness at earlier times than SMASH. In practice, the K^+/π^+ ratio versus p_T is a sensitive observable for tracing the origin of transverse collective behavior and constraining strangeness-production mechanisms in the baryon-rich regime.

The qualitative behavior of K^-/π^- with p_T (panels (e) of Figs. 11−13) is similar to that of K^+/π^+, but with smaller absolute values because K^- are less abundant. The ratio is small at 6 GeV and rises gradually with p_T; at 7 and 8 GeV, the intermediate-p_T enhancement is more evident, particularly for EPOS-LHC and EPOS-4. The models differ quantitatively: both EPOS frameworks predict significantly larger K^-/π^- at intermediate p_T, due to more pair production and less in-medium absorption of K^- than in SMASH. SMASH predicts weaker K^- spectra and therefore a weaker K^-/π^- dependence on p_T. This ratio isolates the physics of pair production and absorption, and is thus complementary to the K^-/K^+ ratio. It is especially valuable for testing K^- production and survival in baryon-rich matter.

The behavior of the p/π^+ ratio as a function of p_T, as shown in panels (f) of Figs. 11-13 for $\sqrt{s_{NN}} = 6$−8 GeV, is strongly model dependent. At all three collision energies, the ratio increases with p_T in all three models, but the increase is much stronger in SMASH than in the EPOS versions. In the first p_T bin (below about 0.1 GeV/c), EPOS-4 shows a large enhancement of p/π^+, indicating a large number of very soft protons, whereas SMASH and EPOS-LHC yield smaller values in this lowest bin. For p_T at and above 0.15 GeV/c, however, the SMASH values are systematically larger than those of EPOS-LHC and EPOS-4 and rise up to $p_T \approx 2.5$−3.0 GeV/c. The EPOS curves increase only moderately over the same range and do not exceed SMASH. This pattern is observed consistently at 6, 7, and 8 GeV. Overall, the p/π^+ ratio is therefore a highly sensitive observable for distinguishing hadronic transport dynamics in SMASH, which produce relatively more protons in the high-p_T tail, from the hybrid/string dynamics of EPOS-LHC and EPOS-4, which produce more very soft protons with a reduced baryon fraction at higher transverse momentum.

This trend is also consistent across all three energies, confirming that the p/π^+ ratio is an especially sensitive observable for discriminating between hadronic and hybrid/string-based dynamics in the NICA energy domain. In all three models, the ratio increases with p_T, but the magnitude of this increase differs substantially. SMASH exhibits a much steeper enhancement of p/π^+ toward intermediate and high p_T than EPOS-LHC and EPOS-4, while EPOS-4 shows a distinctive excess of very soft protons confined to the lowest p_T bin. The detailed p_T dependence of the p/π^+ ratio remains model dependent, but the very-low-p_T region is influenced by the inclusive

broad-rapidity proton contribution and should not be used alone to identify a particular microscopic scenario. The more populated low- and intermediate-p_T regions provide a more stable basis for model comparison.

In Figs. 4−6(f), the proton transverse-momentum spectra are presented for minimum-bias events without detector-motivated acceptance cuts in rapidity or pseudorapidity. At these low collision energies, fully inclusive spectra can receive a large contribution in the lowest p_T bins from baryon transport (and, depending on the generator record, also from projectile/target remnant-like nucleons), which naturally enhances the near-zero-p_T proton population relative to produced mesons. This is the same low-p_T mechanism that leads to the enhancement of the p/π^+ ratio in the very low-p_T region in the EPOS-4 calculations.

The Λ/π^+ ratio as a function of p_T is displayed in panels (g) of Figs. 11−13, which show that in the intermediate transverse-momentum window, EPOS-4 gives a systematically larger Lambda-to-pion ratio than EPOS-LHC and SMASH. At the same time, EPOS-LHC and SMASH are close to each other, with EPOS-LHC slightly larger than SMASH in most bins. This behavior is observed at all three collision energies investigated ($\sqrt{s_{NN}} = 6$, 7, and 8 GeV). The Λ/π^+ ratio is sensitive to the competition between baryon-production and meson-production mechanisms: at low p_T, the ratio is dominated by thermal production and resonance feed-down, while at intermediate p_T it is sensitive in particular to hadronization dynamics (recombination/coalescence versus string fragmentation) and to the magnitude of the radial collective push experienced by heavier hadrons. The larger intermediate-p_T Λ/π^+ predicted by EPOS-4 therefore indicates that this model produces either a stronger radial push for baryons, a hadronization pattern that favors strange-baryon formation at moderate p_T, or enhanced contributions from sources that feed Lambdas in this p_T region. By contrast, SMASH, a hadronic transport model with particle production dominated by resonance dynamics and hadronic rescattering, lacks strong partonic/coalescence contributions and therefore yields a lower Λ/π^+ at intermediate p_T. EPOS-LHC, which is tuned at much higher energies and has a reduced effective core fraction at these low collision energies, ends up close to SMASH. This clear model separation in the intermediate-p_T Λ/π^+ makes it a promising observable for near-term experiments at NICA and similar facilities: a measurement of Λ/π^+ versus p_T and centrality should provide a decisive test of competing model assumptions for hadronization and baryon transport.

IV. CONCLUSION

This work presents a focused set of predictions for minimum-bias Au + Au collisions at $\sqrt{s_{NN}} = 6, 7$, and 8 GeV using three different modeling philosophies (EPOS-LHC, EPOS-4, SMASH). Our conclusions, based on the simulation output itself, are as follows:

Pions as reference benchmark: Charged-pion rapidity and p_T spectra are nearly identical in EPOS-LHC, EPOS-4, and SMASH at all three energies. With resonance feed-down included, and with the same treatment of resonance kinematics in the codes, pion observables are robust but weakly discriminating: pions are well suited for normalizing yields and probing global conservation laws, but they do not by themselves reveal the presence of partonic collectivity at early times.

Strangeness ($K^{\pm}$, Λ): Strange hadrons are strongly model dependent. EPOS-4 systematically predicts higher midrapidity K^+ and Λ yields and harder K^+ and Λ p_T spectra, indicating enhanced pair/string production and an early transverse push from the core. By contrast, with hadronic resonance-dominated production and strong rescattering, SMASH produces steeper (softer) spectra and more concentrated rapidity distributions in the central region. The K^-/K^+ ratio remains < 1 at these energies, but increases with energy and shows a relatively larger hard-p_T contribution in the EPOS models. These trends make kaon and Λ measurements (p_T spectra and rapidity shapes) among the most sensitive probes of non-hadronic dynamics in the NICA window.

Baryons and baryon/meson ratios: The baryon-to-meson ratios exhibit clear and complementary model dependencies. For the p/π^+ ratio, EPOS-4 shows a strong enhancement in the first p_T bin (very low p_T), and thus a large number of very soft protons, whereas EPOS-LHC and SMASH start from smaller values. For p_T at and above about 0.15 GeV/c, the p/π^+ ratio increases with p_T in all three models, but the increase is much more pronounced in SMASH. As a result, SMASH predicts the largest p/π^+ values at intermediate and high p_T, while both EPOS variants remain lower. For the Λ/π^+ ratio, all three models yield small values at low p_T; the ratio then increases with p_T and reaches the largest values at p_T of around 1.5 – 2 GeV/c in EPOS-4, which is systematically above EPOS-LHC, while SMASH gives the smallest values in this intermediate region. In the highest p_T bins, SMASH is close to, or slightly above, the EPOS predictions. Taken together, these patterns show that EPOS-4 is relatively more favorable for baryon production in the very soft and intermediate-p_T region, whereas SMASH tends to enhance baryons relative to mesons at higher transverse momentum.

Rapidity and $p_T - y$ mapping: Two-dimensional p_T versus rapidity maps reveal model-dependent differences in the populated longitudinal and transverse phase space. The EPOS calculations generally extend to larger p_T and broader rapidity regions, whereas SMASH is more concentrated at low p_T; however, comparisons involving rare strange particles are restricted to regions with continuous

population. These differences are consistent with the distinct string, core–corona, hydrodynamic, and hadronic-transport ingredients of the models, although the present maps alone do not isolate a single microscopic mechanism. The $p_T - y$ distributions therefore provide qualitative guidance on the longitudinal and transverse regions where the model predictions differ, but they do not by themselves uniquely determine the microscopic time or mechanism by which the transverse momentum was generated.

NCQ scaling: When plotted as v_2/n_q versus KE_T/n_q, the identified species show an approximate common trend at low and intermediate transverse kinetic energy. EPOS-LHC exhibits the closest visual grouping among the three models, whereas EPOS-4 and SMASH show larger species-dependent deviations and fluctuations. The scaling is not exact, particularly for strange particles and at large KE_T/n_q, where the statistical uncertainties become substantial. The result is therefore interpreted as a generator-level comparison of approximate scaling quality, not as direct evidence for partonic collectivity.

Experimental recommendations: Future MPD/NICA measurements should report K^+ and K^- spectra and the K^-/K^+ ratio as functions of p_T, with particular emphasis on the statistically accessible low- and intermediate-p_T region below approximately 1.5 GeV/c. Their simultaneous energy and rapidity dependences can constrain associated K^+ production, strange-pair production, K^- absorption, and hadronic rescattering. Rapidity-differential $K^\pm$ and Λ yields should be measured at each collision energy, together with K^+/π^+ and Λ/π^+ as functions of both p_T and rapidity. Higher-statistics double-differential $d^2N/(dp_T\,dy)$ maps for K^- and Λ would directly test the phase-space patterns predicted by the models. Finally, identified-particle elliptic flow should be reported as v_2/n_q versus $(m_T - m_0)/n_q$ for pions, kaons, protons, and Λ baryons using common centrality, acceptance, nonflow-suppression, and event-plane-resolution procedures.

Limitations and Outlook: The present study compares three commonly used codes with their standard physics choices, without data-driven retuning, at NICA energies. Differences between models can be attributed to conceptual physics choices (hadronic transport vs hybrid/string+hydro) and implementation details (resonance lists, hadronic afterburners, hadronization recipes). Future data will need to be analyzed systematically, including studies of centrality, acceptance, and variations in model parameters. Future work will also include (i) a detailed study of centrality dependence, and (ii) variations of hadronization and afterburner setups, to determine which ingredients drive which observables.

In summary, EPOS-LHC, EPOS-4, and SMASH provide substantially different generator-level predictions for several identified-hadron observables in minimum-bias Au + Au collisions at $\sqrt{s_{NN}} = 6 - 8$ GeV. Charged and neutral pions constitute a relatively stable baseline, while kaon and Λ production, baryon transport, strange-particle ratios, and the joint $p_T - y$ phase-space distributions exhibit stronger model dependence. The KE_T/n_q-scaled elliptic-flow comparison shows approximate species grouping in the statistically populated region, with the closest visual grouping in EPOS-LHC; however, the scaling is not universal and becomes statistically inconclusive at large transverse kinetic energy. These predictions should therefore be regarded as exploratory model baselines rather than definitive evidence for a particular microscopic phase. Precise rapidity- and p_T-differential measurements of $K^\pm$, Λ, K^-/K^+, Λ/π^+, two-dimensional strange-particle distributions, and identified-particle elliptic flow will provide important constraints on strangeness production, baryon transport, and collective dynamics in the NICA energy range.

ACKNOWLEDGEMENTS

This research was supported by Princess Nourah bint Abdulrahman University Researchers Supporting Project number (PNURSP2026R106), Princess Nourah bint Abdulrahman University, Riyadh, Saudi Arabia.

APPENDIX A

Figure A1 shows an illustrative benchmark of our results for minimum-bias elliptic flow, comparing our results with published RHIC data in this same energy regime. We compare our model v_2 as a function of p_T at 8 GeV with the minimum-bias (0-80%) Au+Au measurement made by the STAR experiment at 7.7 GeV [54]. The energies are slightly different, and, more importantly, the experimental result is obtained by implementing detector acceptance and analysis selections (including track-quality cuts, a given reconstruction event-plane procedure, and a definition of centrality based on reconstructed charged multiplicity), which is not reproduced in our generator-level workflow. Therefore, this comparison is intended to assess whether the magnitude of the predicted v_2 and its p_T dependence fall within a plausible range for this low-energy regime, rather than to provide a validation tuned to the analysis procedure. Fig. A1 is included in the appendix as a data-oriented cross-check, while the main focus of the paper remains the comparative model systematics at $6 - 8$ GeV and across several identified-hadron observables.

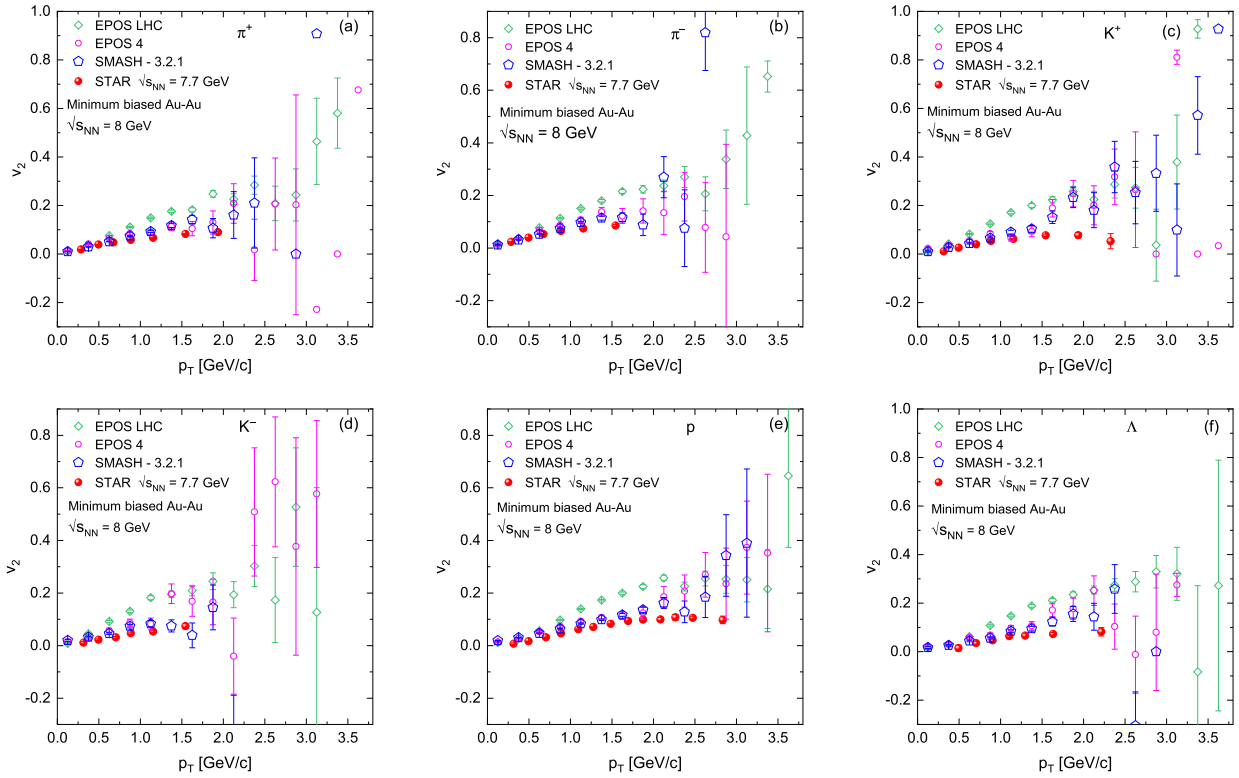


Fig. A1. (color online) Elliptic flow v_2 vs. transverse momentum for minimum bias Au + Au collisions: model results at 8 GeV compared with the minimum bias (0−80%) Au + Au data at 7.7 GeV from the STAR [54]. For the STAR points, the statistical and systematic uncertainties reported by the STAR were combined in quadrature for visualization purposes in this figure. The comparison here is qualitative as the STAR measurement incorporates detector acceptance, track quality selections, event plane reconstruction, and a multiplicity-based centrality definition, which are not used in our generator-level workflow.

References

[1] Y. Aoki *et al.*, Nature **443**, 675 (2006)
[2] S. Borsanyi *et al.*, J. High Energy Phys. **2010**, 73 (2010)
[3] A. Bazavov *et al.*, Phys. Rev. D **85**, 054503 (2012)
[4] J. Adams *et al.*, Nucl. Phys. A **757**, 102 (2005)
[5] K. Adcox *et al.*, Nucl. Phys. A **757**, 184 (2005)
[6] M. Stephanov, Prog. Theor. Phys. Suppl. **153**, 153 (2004)
[7] Z. Fodor and S. D. Katz, J. High Energy Phys. **2004**, 050 (2004)
[8] K. Rajagopal and F. Wilczek, The condensed matter physics of qcd, in *At The Frontier of Particle Physics: Handbook of QCD (In 3 Volumes)* (Singapore: World Scientific, 2001), p. 2061
[9] B. MAGNET, in *Beam Energy Scan II (2018–2019) PHENIX Collaboration White Paper* (New York: BNL, 2014), p. 48
[10] C. Yang *et al.*, Nucl. Phys. A **967**, 800 (2017)
[11] S. V. Afanasiev *et al.*, Phys. Rev. C **66**, 054902 (2002)
[12] H. Collaboration *et al.*, Eur. Phys. J. A **41**, 243 (2009)
[13] D. Blaschke *et al.*, Searching for a qcd mixed phase at the nuclotron-based ion collider facility (nica white paper), 2013.
[14] J. Adamczewski-Musch *et al.*, Eur. Phys. J. A **54**, 85 (2018)
[15] L. Adamczyk *et al.*, Phys. Rev. C **96**, 044904 (2017)
[16] X. Luo, arXiv: 1503.02558
[17] A. Adare *et al.*, Phys. Rev. C **93**, 011901 (2016)
[18] J. T. Mitchell *et al.*, Nucl. Phys. A **904**, 903c (2013)
[19] V. Kekelidze, J. Instrum. **12**, C06012 (2017)
[20] V. Kekelidze *et al.*, Nucl. Phys. A **967**, 884 (2017)
[21] H. I. Alrebdi and M. Ajaz, Nucl. Phys. A **1074**, 123461 (2026)
[22] M. Ajaz and H. I. Alrebdi, Chin. Phys. C (2026), arXiv: 2606.31346
[23] M. Ajaz and H. I. Alrebdi, Eur. Phys. J. Plus **141**, 737 (2026)
[24] M. Badshah *et al.*, Ann. Phys. **492**, 170581 (2026)
[25] T. Pierog *et al.*, Phys. Rev. C **92**, 034906 (2015)
[26] K. Werner, Phys. Rev. Lett. **98**, 152301 (2007)
[27] J. Jahan, *The Beam Energy Scan under the scope of EPOS 4*, PhD thesis (Nantes: Nantes Université, 2022)
[28] K. Werner, Phys. Rev. C **109**, 034918 (2024)
[29] K. Werner *et al.*, Phys. Rev. C **111**, 014903 (2025)
[30] M. Waqar *et al.*, Few-Body Syst. **67**, 16 (2026)
[31] M. Waqas *et al.*, Commun. Theor. Phys. **78**, 045302 (2026)
[32] J. Weil *et al.*, Phys. Rev. C **94**, 054905 (2016)
[33] J. Tindall *et al.*, Phys. Lett. B **770**, 532 (2017)
[34] A. Schäfer *et al.*, Eur. Phys. J. A **58**, 230 (2022)
[35] R. Góes-Hirayama *et al.*, arXiv: 2507.19389
[36] C.-Y. Wong, Phys. Rev. C **78**, 054902 (2008)

[37] I. Bearden *et al*., Phys. Rev. Lett. **93**, 102301 (2004)
[38] C. Sturm *et al*., Phys. Rev. Lett. **86**, 39 (2001)
[39] C. Fuchs, Prog. Part. Nucl. Phys. **56**, 1 (2006)
[40] C. Alt *et al*., Phys. Rev. C **77**, 024903 (2008)
[41] A. Förster *et al*., Phys. Rev. C **75**, 024906 (2007)
[42] H. Appelshäuser *et al*., Phys. Rev. Lett. **82**, 2471 (1999)
[43] E. Andersen *et al*., J. Phys. G: Nucl. Part. Phys. **25**, 181 (1999)
[44] F. Antinori *et al*., J. Phys. G: Nucl. Part. Phys. **32**, 427 (2006)
[45] J. Rafelski and B. Müller, Phys. Rev. Lett. **48**, 1066 (1982)
[46] C. Alt *et al*., Phys. Rev. C **78**, 034918 (2008)
[47] E. Schnedermann, J. Sollfrank, and U. Heinz, Phys. Rev. C **48**, 2462 (1993)
[48] F. Antinori *et al*., J. Phys. G: Nucl. Part. Phys. **30**, 823 (2004)
[49] R. Hagedorn, Nuovo Cimento, Suppl. **3**, 147 (1965)
[50] J. Aichelin and K. Werner, Phys. Rev. C **79**, 064907 (2009)
[51] A. M. Poskanzer and S. A. Voloshin, Phys. Rev. C **58**, 1671 (1998)
[52] C. Alt *et al*., Physical Review C —Nuclear Physics **73**, 044910 (2006)
[53] B. Abelev *et al*., Phys. Rev. C **88**, 044910 (2013)
[54] L. Adamczyk *et al*., Phys. Rev. C **88**, 014902 (2013)